# INVESTIGATIONS INTO THE MECHANISM OF OROTIDINE 5'-MONOPHOSPHATE DECARBOXYLASE: SOURCES OF SUBSTRATE DESTABILIZATION AND TRANSITION STATE STABILIZATION

BY

VANESSA ALEXANDRA IIAMS

THESIS

Submitted in partial fulfillment of the requirements
for the degree of Master of Science in Chemistry
in the Graduate College of the
University of Illinois at Urbana-Champaign, 2010

Urbana, Illinois

Advisor:

Professor John A. Gerlt

ABSTRACT

Orotidine 5′-monophosphate decarboxylase (OMPDC) achieves a rarely paralleled rate acceleration, yet the catalytic basis prompting this enhancement have yet to be fully elucidated. To accomplish decarboxylation, OMPDC must overcome the high energy barrier due to the localized anionic charge of the intermediate. Mechanistic studies employing enzyme mutagenesis and product or intermediate analogues were used to investigate possible transition state stabilization by a carbene resonance structure. Viability of the carbene structure depends upon a key hydrogen bond between O4 of the substrate and the amide backbone of a conserved serine or threonine. Substitution of the conserved residue with Pro resulted in a $k_{cat}/K_M$ of 1 $M^{-1}s^{-1}$; deletion of the FUMP O4 resulted in a product analogue that does not undergo H6 exchange or inhibit decarboxylation. Hence, indirect evidence reveals the O4-backbone interaction plays an important role for binding and catalysis.

OMPDC likely has honed multiple mechanisms to attain its remarkable catalysis. The successful crystallizations of OMPDC a decade ago sparked hypotheses that structure and sequence conserved residues induced productive strain on the substrate-enzyme complex. Here, we demonstrate a new source of stress: a hydrophobic pocket adjacent to the OMP carboxylate that exhibits kinetic parameters characteristic of substrate destabilization. Substitution of these residues with hydrophilic side-chains, by providing hydrogen-bonding partners, decreased $k_{cat}$ by 10 to $10^4$ –fold. The same substitutions display very little change in the rate of product H6 exchange, supporting that this hydrophobic pocket affects the substrate-enzyme complex before the transition state. We also provide evidence that hydrophilic residues can insert water molecules into the pocket with detrimental effects to catalysis.

TABLE OF CONTENTS

CHAPTER 1: INTRODUCTION

Orotidine 5'-monophosphate decarboxylase (OMPDC) catalyzes substrate decarboxylation with a rate acceleration of $10^{17}$, one of the largest catalytic enhancements ever measured for a cofactor-less enzyme (Fig.1).[1] However, the source of acceleration is much debated; it is uncertain how OMPDC can speed decarboxylation without a cofactor or metal ion to stabilize an intermediate that most likely involves a localized carbanion.

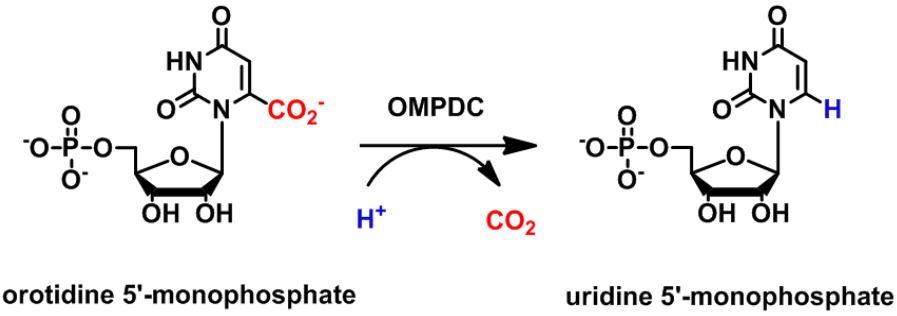


**Figure 1**: Reaction catalyzed by OMPDC.

OMPDC operates in the *de novo* pyrimidine nucleotide biosynthetic pathway by converting orotidine 5'-monophosphate (OMP) into uridine 5'-monophosphate (UMP) with downstream pathways leading to thymine and cytosine nucleotides. Most organisms also have a salvage pathway that recycles pyrimidine nucleosides, but some eukaryotic organisms such as *Plasmodium falciparum*, the causative agent of malaria, utilize only the *de novo* pathway. Attempts to exploit this disparity by selectively knocking down the *de novo* biosynthesis have encouraged the development of OMPDC inhibition studies for medicinal studies, but also for mechanistic work that could identify the enzymatic bases for catalysis. Inhibition studies have shed light on the properties of the active site and ligand binding: Most binding candidates alter functionalities of the pyrimidine head or replace it altogether, as contacts to the O2' and O3' ribose hydroxyl and the phosphate dianion moiety are critical to binding, but not directly to

catalysis. Deletions of the OMP ribose hydroxyl groups that form substrate-enzyme hydrogen bonds or mutations of their enzyme partners D20 or T79* (*Methanothermobacter thermoautotrophicus* numbering, where the asterisk indicates a residue from the second subunit) cause up to a $10^3$ reduction in $k_{cat}/K_M$.[2] Removal of the phosphate dianion reduces catalysis by almost $10^5$-fold.[3]

Many of the ligands examined for binding hint at the pathway and bases important for catalysis. The discovery of the extraordinarily tight affinity of OMPDC for 6-hydroxyUMP (BMP) is attributed to transition state-like binding, substantiating that the catalyzed pathway uses an anionic intermediate.[4] Analogues that also contain electron density around C6, 6-azaUMP and 6-aminoUMP, showed sub-micromolar inhibition values that further bolstered the claim that the reaction proceeds through a carbanion. Negatively charged, but bulkier, ligands such as sulfonoUMP, 5,6-dihydroOMP, and 6-phosphonoUMP (although lacking independent verification) have been reported to bind to the enzyme, suggesting that the active site accommodates large, negatively charged substituents at C6.[5-7] These inhibition values led to claims that the enzyme structure stabilizes out-of-plane C6 groups. Analogues substituted at C5 with halogen and cyano groups and dihydroOMP have led to speculation about a putative "$CO_2$ binding pocket" in the active site. Inhibition studies in conjunction with sequence alignments highlight the conservation of active site architecture and residues that interact with the substrate.

In spite of conserved active site residues and geometry, OMPDC sequences are highly divergent (less than 10% sequence identity within the family) and split into four major subfamilies identified by sequences and the length of the loop at the end of the $7^{th}$ β strand, which closes off the active site during catalysis.[8] Although overall sequence identity can be very low, all OMPDCs fold into a dimer of $(\beta/\alpha)_8$ barrels with precisely placed and highly conserved

active site residues. Mechanistic hints can be found from the conserved protein sequence and structure. Each active site is located at the interface of the dimer and requires residues from both subunits for activity. These conserved residues include D70, K72 and D75* of the DxKxxD motif; D20 and K42 that form part of the ribose binding domain; and S127, Q185 and R203 that bind the pyrimidine and phosphate dianion. The conserved residues participate in the extensive hydrogen bonding and/or charged network lining the active site and assist in catalysis. Mutagenesis of any of these residues results in sizeable reductions in $k_{cat}/K_M$, if not near inactivation as in the case of K72.[2,9,10]

The uncatalyzed reaction is calculated to have a rate of $10^{-16}$ $s^{-1}$, which translates to a half-life of 78 million years.[1] This sluggish rate results from the instability of the anionic intermediate because of the lack of resonance stabilization or an electron sink (Fig 2a). OMPDC, however, does not provide an obvious source of stabilization or reduction of the activation barrier. Consequently, how OMPDC can considerably increase turnover without a cofactor is of great interest and has generated a number of mechanistic proposals.

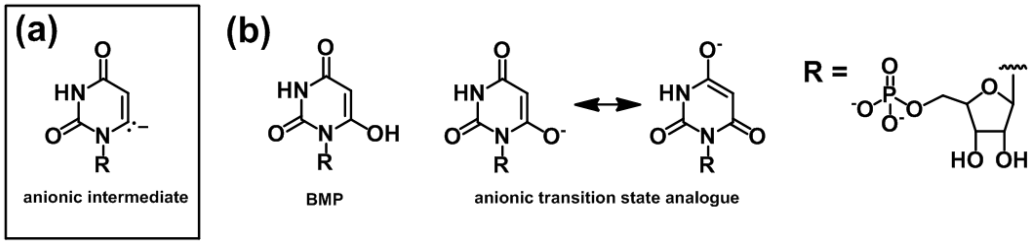


**Figure 2**: (a) Putative anionic intermediate with negative charge localized at C6. (b) Structure of BMP inhibitor. Resonance between O4 and O6 of BMP mimic possible transition state delocalization.

Silverman and Groziak proposed an addition-elimination reaction in which a nucleophile on the enzyme forms a covalent bond at C5 and protonates C6 (Fig. 3a).[11] Concurrent loss of the

carboxylate as carbon dioxide and the nucleophile would yield product UMP without the formation of an anionic intermediate. However, no kinetic isotope effect was observed for isotopically labeled 5-$^{13}$C or 5-$^{2}$H OMP, eliminating nucleophilic attack at C5 as the mechanistic pathway.[12,13]

Another proposal put forward a concerted protonation and decarboxylation that would bypass the generation of a high energy anionic intermediate (Fig. 3b).[14,15] $D_2O$ solvent kinetic isotope effects and $^{13}$C labeled carboxylate kinetic isotope effects showed that decarboxylation, determined to be the rate-limiting step, was separate from protonation.[13,16] In 50/50 $D_2O/H_2O$ the measured product isotope effect is unity (i.e. equivalent amounts of protonated and deuterated product were observed spectroscopically), providing further evidence that protonation does not help initiate nor is concurrent with the rate determining step.[17] Additionally, a $10^2$ -fold rate enhancement of decarboxylation and H6 exchange for 5-fluoroOMP and 5-fluoroUMP indicate an anionic intermediate that is stabilized by the inductively electron withdrawing fluorine (Fig. 2b).[12] Overall, accumulated experimental evidence favors a two step reaction with a negatively charged intermediate over the concerted reaction.

Several propositions utilized protonation as a means to stabilize the anionic charge of the intermediate since. Beak and Siegel suggested a zwitterionic or ylide mechanism where protonation of O2 yields a positively charged quaternary amine at N1 that could inductively stabilize the neighboring negative charge on C6 (Fig. 3c).[18] A similar zwitterionic intermediate is found in thiamin pyrophosphate-catalyzed reactions. Lee and Houk proposed a similar delocalization scheme in which the anionic intermediate forms a carbene resonance structure with charge delocalized to O4 (Fig. 3d).[19] Their proposal suggested that a conserved lysine, aided by a hydrophobic protein interior, transfers a proton to O4 to yield a neutral intermediate.

It was also noted that the transition state analogue 6-hydroxyUMP (BMP, Fig. 2b), a remarkably strong inhibitor with a $K_i$ of $9x10^{-12}$ $M^{-1}$ for yeast OMPDC, not only mimics the anion at C6, but can also generate an anion at O4 similar to the Lee and Houk intermediate (Fig. 2b). However, in 2000 four crystal structures of OMPDC, from *E. coli, M. thermoautotrophicum, S. cerevisiae,* and *P. falciparum*, were published simultaneously.[14,20-22] O2 and O4 form hydrogen bonds with the enzyme and play an important role in binding and in orientation of the substrate. However, the crystal structures showed that neither O2 nor O4 have nearby acidic proton donors, signifying that neither oxygen becomes fully protonated. $^{15}N$ kinetic isotope effect studies performed with the $^{15}N$-labeled picolinic acid show no bond order change, which contradicted the formation of a quaternary ammonium intermediate at or before decarboxylation, and was the final death knell for the zwitterionic mechanism.[23]

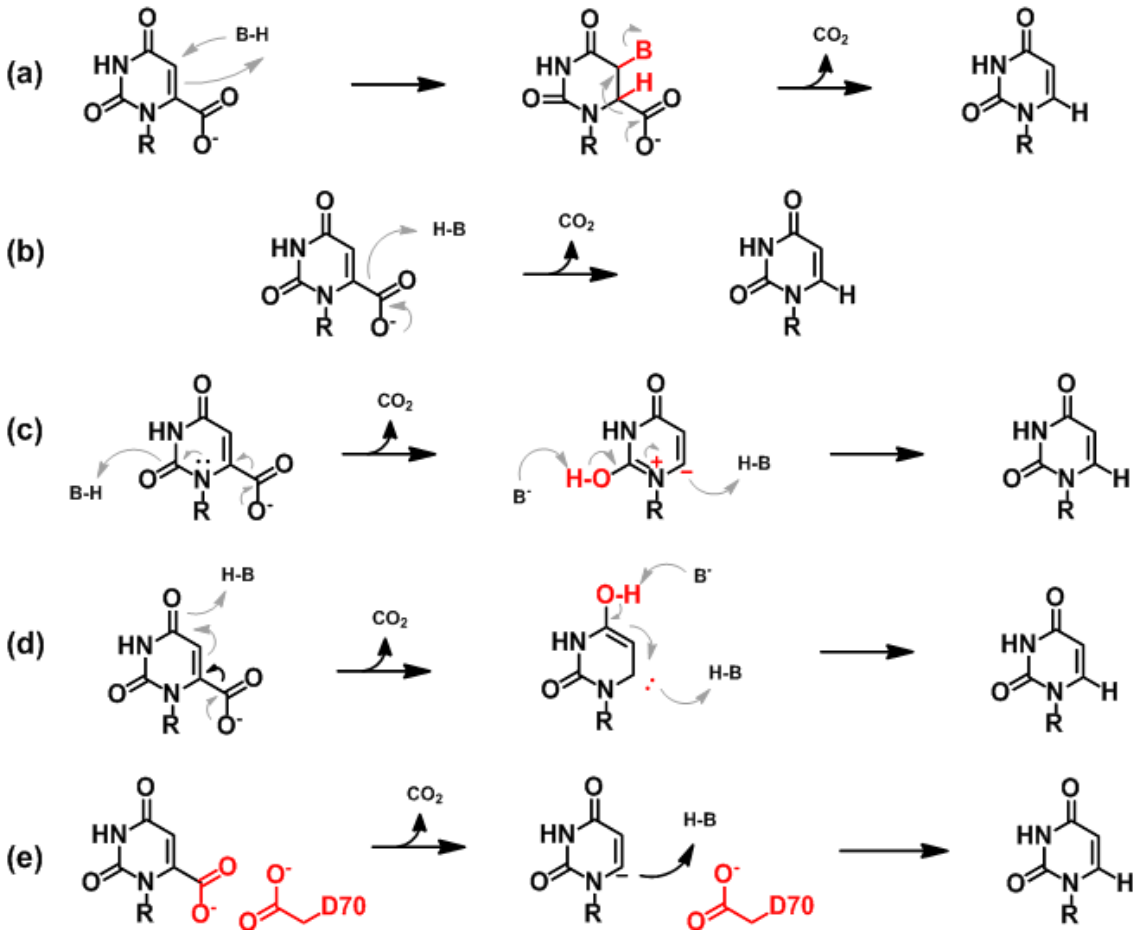


**Figure 3**: Mechanistic schemes for OMPDC-catalyzed decarboxylation without generation of a unstabilized, high-energy intermediate. The main features of each proposal are highlighted in red. (a) Addition across the C5-C6 double bond followed by simultaneous decarboxylation and elimination of the nucleophile. (b) Concerted decarboxylation and protonation. (c) Ylide/zwitterionic intermediate facilitated by protonation at O2. (d) Carbene mechanism instigated by protonation at O4. (e) Ground state or substrate destabilization due to interactions between the OMP carboxylate and the nearby D70 charge.

The 100+ currently deposited crystal structures of OMPDC reveal that the residues of the conserved DxKxxD motif point toward the C6 carboxylate group. The functional significance of

the two conserved aspartates is unclear, and this discovery prompted Wu *et al*. to suggest that OMPDC utilizes ground state destabilization.[21] The concept of ground state destabilization originates from the Circe effect introduced by Jencks.[24] Wu *et al.* proposed that the positively charged lysine "entices" the substrate carboxylate into the proper active site conformation, but the neighboring negatively charged aspartates provide electrostatic stress that encourages decarboxylation (Fig. 3e). The strain is felt only by the Michaelis-Menton complex, thereby decreasing ΔΔG between the ground state and transition state. However, the hypothesis for ground state destabilization was countered by Florian *et al*., who responded that desolvation costs outweigh destabilization benefits.[25] Although $k_{cat}$ would increase with heightened hydrophobicity, desolvation would increase $K_M$ and consequently $k_{cat}/K_M$ would not improve.

Ground state destabilization of the enzyme-substrate complex could utilize conformational changes to position the conserved aspartates effectively. The costs of desolvation or structural changes towards a catalytic conformation could be compensated by the intrinsic binding energy of the phosphate group. OMPDC decarboxylates the orotidine analogue 1-(erythrofuranosyl)orotic acid (EO) very slowly—$k_{cat}/K_M$ is 2.1 x $10^{-2}$ $M^{-1}s^{-1}$.[3] In the presence of phosphite dianion, EO decarboxylation accelerates almost $10^5$-fold. Restoration of the phosphoryl moiety reconstitutes the original OMP kinetics, provided that the entropic effect of binding two substrate pieces is taken into account. Catalytic activation by the addition of phosphite supported the "Jencksian" concept that enzymes redirect binding energy to "pay" for catalysis.[24]

In spite of extensive interrogation, the drive behind OMPDC catalysis is not completely clear and remains contentious. In reality the enzyme probably uses multiple elements to decarboxylate OMP, of which two possible mechanisms are described herein: carbene-like

resonance facilitated by hydrogen bonding—rather than proton transfer—and hydrophobic destabilization of the OMP carboxylate group. Mechanistic hypotheses explored in this thesis examine OMPDC from *M. thermoautotrophicus* as a model enzyme.

# CHAPTER 2: INVESTIGATION OF POSSIBLE TRANSITION STATE STABILIZATION BY CARBENE-LIKE RESONANCE STRUCTURES

## 2.1 BACKGROUND

The discovery of the exceptional rate enhancement of OMPDC prompted a proliferation of proposals regarding the enzymatic stabilization of the carbanion intermediate. Houk and Lee suggested that the charge at C6 of the anionic intermediate delocalized onto O4 where it was stabilized by protonation.[19] They calculated that the activation energy of the reaction was lowered by 28 kcal/mol if O4 were protonated, provided a proton donor was located nearby in a sufficiently hydrophobic environment to tune acceptor and donor $pK_a$s. Because sequence comparisons showed an absolutely conserved lysine, Houk and Lee suggested that the acid catalyst was this lysine ($pK_a$~8), which would require assistance to protonate a carbonyl ($pK_a$~0.5). Hence $pK_a$ tuning was invoked *via* a hydrophobic interior.[19,26] With O4 protonation, C6 reorganizes into a neutral carbene with the lone pair residing in an $sp^3$ orbital.

However, subsequent crystallographic structures revealed the lack of a plausible proton donor near O4. Instead, O4 forms hydrogen bonds to the backbone amide of S127 and to a conserved water molecule. Although less advantageous than full protonation, OMPDC likely engages the O4-backbone amide bond to bind and help stabilize charge from C6. Computational analysis shows that charge is not on C6 alone, but spread throughout the pyrimidine ring.

Gene sequences and available crystal structures show that S127 and the amide-O4 bond are highly conserved in orthologous OMPDC enzymes as serine or threonine.

```
BACsu.7245429.1DBT    R P S L I A V T Q L T S T S E Q I M K D E L L I
LISmo.224501367       R P K I I A V T Q L T S T S E T D M Q T E Q L I
GEOka.261375801       R P R C I A V T Q L T S T D E R M L H E E L W I
STRpn.15902657        - - K L I A V T Q L T S T S E A Q M Q E F Q N I
ENTfa.29376265        V P E L I A V T Q L T S T S E E E M H H D Q L I
ESCco.20151198.1L2U   A P L L I A V T V L T S M E A S D L V D L G - M
SALen.261246897       A P L L I A V T V L T S M E T S D L H D L G - V
PSEae.15598072        R P L L I G V T V L T S M E R E D L A G I G - L
HELpy.15644639        - P L I M G V S A L T S F S E E - - E F L M V Y
SACce.241913356.3GDL  - R G L L M L A E L S C K G S L A T G E Y T K G
HOMsa.226438251.3EX4  - R G C L L I A E M S S T G S L A T G D Y T R A
NEUcr.85076080        D R G L L I L A Q M S S K G C L M D G K Y T W E
METth.7546203.1DV7    - R E V F L L T E M S H P G A E M F I Q G A A D
AERpe.14602012        - - - L V L V V S M S H P G S R E V L D P C L D
                                .   :     : :
                      117             127             137
```

**Figure 4**: Sequence alignment illustrating high conservation of S127 as serine or threonine among archeal, bacterial and eukaryotic OMPDC enzymes (ID includes genus and species name abbreviations, gi number, and pdb file). Crystal structures confirm that OMPDC orthologues utilize theonines and not the adjacent serines in amide-O4 bonds (pdb files 1DBT and 1L2U).

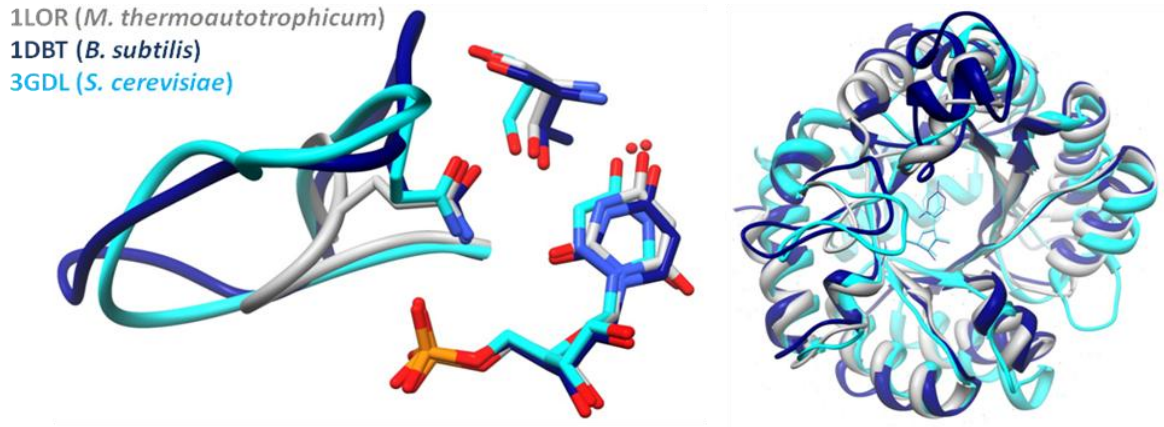


**Figure 5**: S127 analogues and loop after the 7$^{th}$ β strand, which caps the active site. The architecture and placement of key residues remain constant across the domains despite sequence divergence. Archeal *M. thermoautotrophicus* S127 and Q185 liganded with BMP (gray), bacterial *B. subtilis* T123 and Q194 with UMP (navy blue), eukaryotic *S. cerevisiae* S154 and Q215 with 6-azaUMP (cyan).

Because the hydrogen bonds formed between substrate and the S127 backbone and side chain are highly conserved and potentially enhance catalysis, the effects of hydrogen partner deletion by site-directed mutagenesis and substrate analogues were investigated.

## 2.2 RESULTS AND DISCUSSION

*S127 Enzyme Mutagenesis.* Mutational analysis of S127 underlines the magnitude of its catalytic or binding role. The importance of S127 lies in its dual hydrogen bonds: besides the bond between the OMP O4 and the S127 backbone amide, the hydroxyl side-chain of S127 bonds to N3 of the substrate and to another highly conserved residue, Q185, which in turn coordinates O2 and R203, a key phosphate binding residue (Fig. 6a). S127 and Q185 together "clamp" the substrate into the active site, however, deletion of the serine side-chain (5.7 kcal/mol) is effectively equivalent to the double deletion of both the serine and glutamate side chains (6 kcal/mol). The magnitude of the S127 mutation demonstrates the major role of the S127 hydrogen bonds in organizing the active conformation of the active site. The absence of enzyme contacts to O2, N3, and/or O4 of the pyrimidine ring of OMP probably hampers correct conformational binding, as illustrated by S127A co-crystallized with UMP: instead of the expected *syn* conformation, UMP binds in an *anti* conformation with O2 adjacent to the DxKxxD motif (i.e. the pyrimidine ring is flipped 180°).[27] Yet, S127 mutants exhibit both increases in $K_M$ and decreases in $k_{cat}$ suggesting that the clamp is not limited to binding or substrate specificity, but also participates in transition state stabilization.

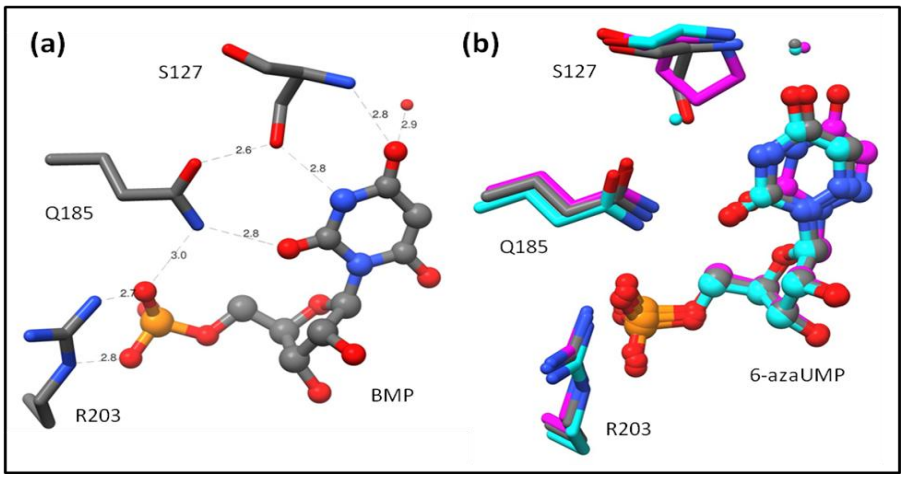


**Figure 6**: Active site clamp showing (a) hydrogen bonding network between BMP and clamping residues and (b) structural similarities and differences in the same residues between WT (gray), S127G (cyan) and S127P (magenta). Waters are color coded to match structure colors.

The $k_{cat}$ for S127A is reduced by 100-fold, while $K_M$ is increased to 70 μM, yielding a second order rate constant $k_{cat}/K_M$ of 5 x $10^2$ $M^{-1}s^{-1}$ (Table 1). This effect comes solely from the absent hydroxyl group and not from perturbation of the O4-amide backbone bond. S127G also displays impaired kinetic parameters, but appears to be partially rescued by a water molecule observed in the crystal structure (Fig. 6b). Because the water can fulfill some of the hydrogen bonding requirements, S127G consequently has a higher $k_{cat}/K_M$ than S127A. However S127P, although it minimally alters the active site architecture, experiences an additional 800-fold reduction in $k_{cat}/K_M$ compared to S127A. The effect of S127P compounds the deletion of S127 hydrogen bonds to both O4 and N3, of which the extra 800-fold reduction in $k_{cat}/K_M$ derives from the missing O4-amide bond. Although the amide backbone cannot be mutated as easily as side-chains are, the differential between the alanine and proline mutants show that the O4-amide interaction contributes at least ~ 4 kcal/mol to catalysis. S127P catalysis with an alternate substrate, FOMP, yields a $k_{cat}/K_m$ of 1.4 x$10^2$ $M^{-1}s^{-1}$. Based on impaired OMPDC mutants D70G

and D70N, the 5-fluoro substitution increases $k_{cat}/K_M$ by 300 to 400-fold; S127P decarboxylates FOMP about 140-fold faster than OMP, which confirms the poor kinetic ability of S127P.[10]

| OMPDC | $k_{cat}$ ($s^{-1}$) | $K_M$ (μM) | $k_{cat}/K_M$ ($M^{-1}s^{-1}$) |
|---|---|---|---|
| WT | 4.0 | 2.0 | $2.0 \times 10^6$ |
| S127A | 0.049 | 62 | $7.9 \times 10^2$ |
| S127G | 0.28 | 92 | $3.0 \times 10^3$ |
| S127P | - | - | 1 |

**Table 1**: Kinetic parameters for S127 mutants of Mt OMPDC.

*3-DeazaUMP Inhibition*. I synthesized a product analogue, 3-deazaUMP, which lacks N3 of the uracil ring (Fig. 7). It acts as the complementary "product mutant" to the S127A and S127G enzyme mutants, i.e. all of them exclusively eliminate the N3-S127 hydroxyl hydrogen bond. Therefore wildtype OMPDC with 3-deazaUMP and S127A mutant with OMP should exhibit comparable effects on ligand binding affinity. The mutant S127A, assuming $K_M$ approximates $K_d$, has a substrate binding affinity of 70 μM, which is almost 50-fold higher than wildtype. Based on S127A kinetics, deletion of the UMP N3 moiety ought to result in 50-fold weaker binding since the enzyme-substrate complex loses the same hydrogen bond. However, between pH 6 to 9, 3-deazaUMP has a $K_i$ of 50 μM, which is about 4-fold lower than UMP $K_i$.

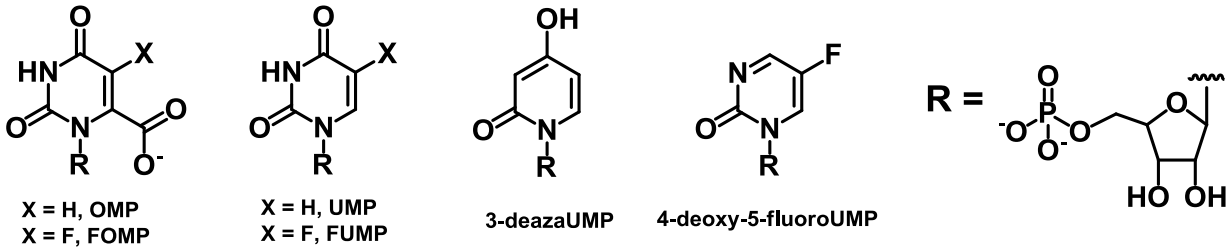


**Figure 7**: OMPDC substrates (OMP, FOMP), products (UMP, FUMP) and analogues lacking key contacts involved in enzyme binding, N3 and O4 of the pyrimidine ring.

| "Intact" Piece | Interacting Partner | $K_i$ (μM) | Difference |
|---|---|---|---|
| OMP | + WT OMPDC | 1.5 | Increase |
| | + S127A OMPDC | 70 | 50-fold |
| WT OMPDC | + UMP | 200 | Decrease |
| | + 3-deazaUMP | 50 | 4-fold |

**Table 2**: Enzyme and product mutation that deletes a hydrogen bonding partner of the N3-S127 interaction shows opposite trends. A consequence of N3 deletion causes 3-deazaUMP to have an elevated O4 $pK_a$ value, which may yield the disparity between apparent $K_i$ trends. Provided that OMPDC could similarly modulate O4 $pK_a$ during the reaction, the enzyme could exploit the enhanced hydrogen bonding for intermediate stabilization.

The incongruity between 3-deazaUMP binding affinity and S127A binding affinity might reflect the potency of the O4-backbone hydroxyl interaction (Table 2). The loss of affinity due to the absent N3-hydroxyl interaction might be compensated by a strengthened O4-backbone amide interaction that is facilitated by shifts in O4 $pK_a$; 3-deazaUMP matches the $pK_a$ of the backbone amide better than UMP since the $pK_a$ of the 3-deazaUMP hydroxyl (ca. 6.5) is much larger than the orotate carbonyl $pK_a$ (ca. 0.5).[26,28] Additionally, at the decarboxylation reaction pH 7.1, the majority of 3-deazaUMP inhibitor exists in an ionized state, thus the oxyanion charge, although partially delocalized onto O2, might further enhance hydrogen bonding. If the enzyme were capable of such O4 $pK_a$ tuning between ground and transition state, increasing hydrogen bond strength during the transition state would preferentially stabilize the high-energy intermediate and accelerate catalysis. Further investigation with the substrate analogue 3-deazaOMP or 3-deazaBMP and 6-aza-3-deazaUMP inhibitors might clarify the interplay between weakened N3 interactions and possibly strengthened O4 interactions.

*Exchange of 4-Deoxy-5-FluoroUMP.* 4-Deoxy-5-fluoroUMP (DFUMP, Fig. 7) was synthesized according to Driscoll *et al*.[29] However, no exchange of H6 of DFUMP in enzyme concentrations up to12 mg/mL was observed by $^{19}$FNMR over a period of 15 days. One explanation is that OMPDC requires O4 for transition state stabilization and its absence demolishes exchange activity. Measuring exchange, however, is complicated by the apparent degradation of DFUMP at high concentrations of enzyme.[*] Addition of 0.25 equivalents of DFUMP inhibited FUMP exchange only 3-fold, showing that DFUMP can only weakly compete with FUMP binding. Thus in addition to any catalytic incompetence, DFUMP poorly binds to the active site.

## 2.3 CONCLUSIONS

Deletion of O4 from OMP, alteration of its hydrogen bonding strength, or mutation of the enzyme partner S127 shows that O4 is extremely important for binding and catalysis. Clearly O4 plays a significant role in substrate and product binding as evinced by the lack of exchange inhibition by DFUMP or of DFUMP exchange itself. The product analogue 3-deazaUMP suggests the capacity of the O4-backbone amide interaction for strong hydrogen bonding, since it appears to partially rescue N3-hydroxyl deletion. Side-chain and backbone mutations to S127 have both large $k_{cat}$ and $K_M$ effects. However, whether the O4-backbone interaction actually increases during catalysis to lower transition state free energy is still unclear.

[*] DFUMP in high concentrations of enzyme was observed to degrade over 2 weeks as seen by decreasing intensity of DFUMP peaks in $^{1}$HNMR and $^{19}$FNMR spectroscopy). Slow glycosidic cleavage was also observed by Carlow *et al.* with DFUMP in the presence of cytosine deaminase and was attributed to minute enzyme impurities.

# CHAPTER 3: INVESTIGATION OF THE CONTRIBUTION OF THE HYDROPHOBIC $CO_2$ POCKET TO SUBSTRATE DESTABILIZATION

## 3.1 BACKGROUND

Hydrophobic interactions have long been recognized in guiding protein folding and enhancing substrate specificity. Enzyme active sites might also employ hydrophobic residues in catalysis to manipulate $pK_a$ values or the energetics of nearby charged groups. Strategically placed nonpolar sites have been previously conjectured for some enzyme chemistries such as thiamin pyrophosphate cofactor-dependent reactions. Non-enzymatic decarboxylation of pyruvate to acetylaldehyde occurs$10^4$-$10^5$ times faster in ethanol than in water when in the presence of thiamin derivatives.[30] Other works showed that pyruvate dehydrogenase binds the neutral transition state analogues thiamin thiazolone pyrophosphate and thiamin thiothiazolone pyrophosphate over positively charged forms by a factor of at least 20,000.[31] The solvent effects and inhibition by transition state analogues implicate active site hydrophobicity in these thiamine-dependent enzyme reactions. Enzymes such as pyruvate dehydrogenase and pyruvate decarboxylase may bind thiazolium groups in a hydrophobic region to disfavor charged species and drive the reaction toward a favorable neutral intermediates.

OMP decarboxylation, which removes a negative charge in generating the UMP product, is another candidate for hydrophobicity-assisted catalysis. Experimental and computational work have shown that decreasing solvent polarity or the dielectric constant of the reaction increases the rates of OMP decarboxylation.[19,32] The results support hydrophobic environments that favor neutral structures over charged molecules, e.g,. greasy interiors that prefer UMP to OMP or K72 as an amine rather than an ammonium cation. Non-enzymatic decarboxylation of orotate derivatives in organic solvents have shown 10 to $10^3$-fold enhancements versus the aqueous

reaction, presumably by increasing the free energy of the reactants and consequently decreasing the activation barrier.[32] However, for $k_{cat}$ to increase, this interpretation assumes the anionic intermediate free energy is not equally elevated by the solvent hydrophobicity; possibly delocalization of the intermediate charge throughout the ring helps stabilize the intermediate. The reaction rate increase in organic solvents shows a strong negative correlation to the solvent acity (anion solvating tendency), illustrating that aprotic environments improve decarboxylation versus protic or solvating environments. Similarly, the enthalpy of orotate decarboxylation modeled with an ammonium cation proton source was dramatically dependent on dielectric constant, ε: in water (ε = 78), both the experimental and calculated enthalpy of reaction is 42 kcal/mol, but the enthalpy in a hydrophobic enzyme interior (estimated ε = 4) is a calculated 23.9 kcal/mol lower.[19]

As has been pointed out in computational analyses, catalysis based on the desolvation of the substrate would be associated with a large free energy cost (est. 32 kcal/mol) that may exceed the binding energy provided by the phosphate group (approximately 11-12 kcal/mol).[25,32] The unfavorable energetics of eliminating hydrogen bonds could override the benefits of catalysis driven by hydrophobic effects. Additionally, the substrate is enveloped by an extensive hydrogen bonding network that suggests that the active site is largely polar rather than nonpolar. However, a hydrophobic region within the active site might reap the catalytic benefits of hydrophobicity without paying the full price of desolvation.

A related mechanism, electrostatic repulsion, which also destabilizes the substrate, has been investigated. Typically, OMPDC kinetics are measured via decarboxylation; however, enzyme activity can be examined in terms of exchange of H6 on the pyrimidine ring (Fig. 8a). The enzyme active site decreases the $pK_a$ of UMP by at least ten $pK_a$ units, enabling

exchange.[10,33] Both decarboxylation and exchange engender the anionic intermediate, and, therefore, both are expected to utilize the same transition state stabilization mechanisms; any enzyme functionality that contributes to transition state stabilization should have equal effects on decarboxylation and exchange rates. However, only substrates with C6 carboxylates experience pre-transition state interactions, thus only decarboxylation could undergo destabilization (Fig. 8b). Consequently, changes in $k_{cat}$ minus changes in $k_{ex}$ reflect effects due to diminished destabilization.

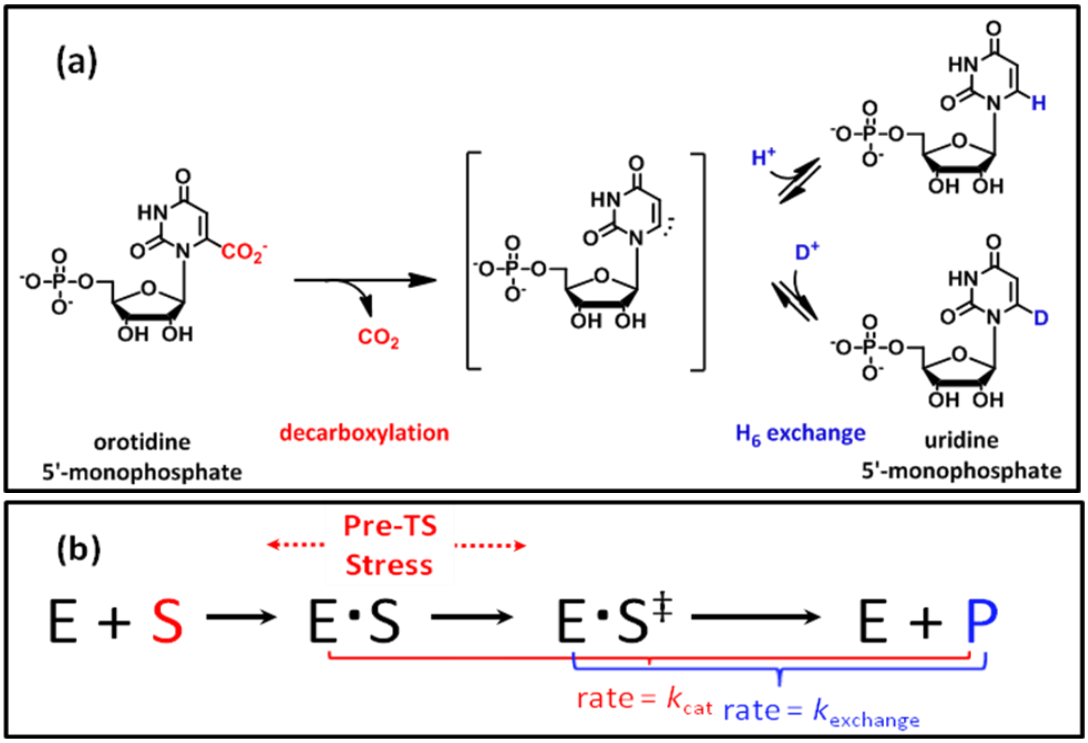


**Figure 8**: Decarboxylation (red) and H6 proton exchange (blue) reactions for OMPDC. Both reactions proceed through the anionic intermediate (‡), but only decarboxylation is subject to pre-transition state (pre-TS) strain.

Work performed by Chan *et al*. showed that mutagenesis of the first aspartate (D70) of the DxKxxD triad to asparagine or glycine exhibited decarboxylation rates reduced by 100 to

1000-fold, but had no effect on the rate of FUMP exchange.[10] This suggests a catalytic mechanism important to decarboxylation but not accessed in the transition state. D70 might selectively contribute electrostatic and steric stresses that increase the free energy of the enzyme-bound substrate, but not the intermediate. In conjunction with electrostatic repulsion, a hydrophobic environment could also contribute to catalysis via destabilization of the enzyme-substrate complex. The effects of hydrophobicity, which are presented in this thesis, can be similarly investigated by a comparison of OMPDC catalyzed reactions.

Structural data capture possible "stressed" ligands bound in the active site. Catalytically inactive Mt OMPDC K72A and D70A/K72A mutants crystallized with OMP (1km6) and 6-cyanoUMP (2zz2) show the C6 substituents twisted out of the aromatic plane. The active site is apparently able to distort substrate or substrate analogues even with the D70A mutation, possibly by utilizing the water molecules that fill the cavity produced by alanine substitutions. These structures may point to an enzyme active site that is designed or predisposed through steric and/or electronic effects to favor distortion of C6 substituents. For instance, a hydrogen bond to K42 might stabilize the twisted carboxylate OMP in 1km6. The surrounding network of other hydrogen bonding residues might orient waters or DxKxxD side-chains to force large C6 substituents out of plane. Serendipitously, activated waters were also shown by crystallization of OMPDC with cyanoUMP: the structure captured the transformation of cyanoUMP to BMP (2zz1), perhaps another indication of an active site able to destabilize C6 functional groups.

Solvent effects, computation, mutagenesis, kinetics and structural work allude to destabilization mechanisms in OMPDC decarboxylation. However, the enzyme could maintain multiple means to accomplish this effect. Electrostatic repulsion primarily by a single residue,

D70, has been demonstrated. Parallel efforts showing hydrophobic destabilization via a greasy "$CO_2$ pocket" are described in the following sections.

## 3.2 RESULTS AND DISCUSSION

Structural and kinetic analyses have uncovered an active site hydrophobic pocket comprised of at least six residues that are adjacent to the C6 carboxylate group of OMP, and which may work in tandem with the highly conserved DxKxxD motif to destabilize the C6 carboxylate. The C6 carboxylate is cradled by the charged triad on one side and hydrophobic pocket residues on the other. Previous crystallographic data and inhibition studies suggest that the polarity and architecture of this region appear to bind "bent" or bulky anionic structures including OMP, cyanoUMP, aminoUMP, dihydroOMP, sulfonoUMP, phosphonoUMP and pyrazofuran monophosphate (although independent analyses have yet to confirm some of these inhibition values).[6,7,21,27,34] Through electrostatic and/or steric effects, the DxKxxD motif might push OMP's carboxylate group into the hydrophobic pocket to accelerate decarboxylation. On the other hand, the pocket residues and the DxKxxD motif might be complementary, but structurally and mechanistically independent, means of destabilization that assist in decarboxylation.

These pocket residues reside on the ends of five β strands of the barrel. Hydrophobic pocket residues consist of I96 ($4^{th}$ β strand), L123 ($5^{th}$ β strand), V155 ($6^{th}$ β strand), I178 and P180 ($7^{th}$ β strand), I200 ($8^{th}$ β strand). The aliphatic chains of K42 and K72 might also contribute to pocket geometry and hydrophobicity. The pocket was investigated with a two-pronged approach to uncover the contribution of the hydrophobic pocket to catalysis. In the first method, I replaced hydrophobic residues with polar serines, threonines or asparagines (Fig. 9).

Increased polarity could stabilize the charge on OMP and disfavor catalysis by lowering the free energy of substrate-bound enzyme complexes before the intermediate.

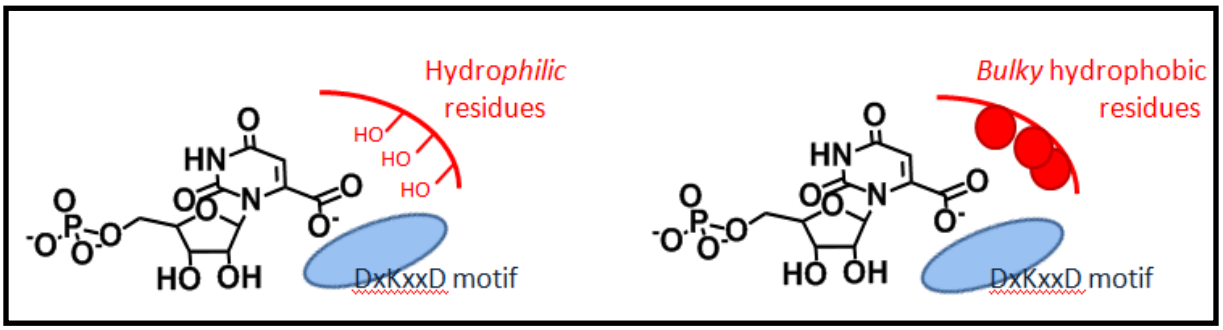


**Figure 9**: Two approaches to identify and/or quantify the contribution of the $CO_2$ hydrophobic pocket. The first consists of hydrophobic residue replacement with hydrophilic residues. The second substitutes large residues into pocket cavity to create a hydrophobic wall.

Residues with polar side-chains produced mutant OMPDCs with $k_{cat}$ values attenuated by 10 to 100-fold, but with virtually no effect for $K_M$ (Table 3). Decarboxylation rates decreases proportionally to polarity. From most detrimental to catalysis to least, aspartate > serine > threonine ~ asparagines. The reductions in $k_{cat}$ substantiate the hypothesis that the pocket residues play some role in catalysis, but do not alter binding affinity or enzyme conformational changes to the closed, active structure. Exchange rates of the H6 proton of FUMP, $k_{ex}$, were typically within a factor of three from wildtype values. FUMP instead of UMP was used to exploit the close, but well differentiated, $^{19}$F-NMR peaks of protonated and deuteriated FUMP and to circumvent the loss of enzyme activity that occurs with protracted UMP exchange. Altogether the kinetic data, similar to the D70 mutagenesis conclusions, indicate that these pocket residues are not involved in binding or transition state stabilization, but do assist decarboxylation by adding strain to the C6 carboxylate. Even more startling, a substitution with an anionic residue, V155D, showed a dramatic 8000-fold decrease in $k_{cat}$, but no effect on $K_M$. In

the context of the total OMPDC acceleration, which increases the rate by $10^{17}$-fold and provides ca. 25 kcal/mol stabilization to the uncatalyzed reaction, exchanging a greasy valine for charged aspartate demolishes nearly 20% of OMPDC catalysis! Contrary to the other mutations, V155D actually appears to slightly increase $k_{ex}$ rates. Surrounded by hydrophobic residues, the $pK_a$ of V155D might be raised and the aspartic acid could provide a protonation source that contributes to the rate of exchange.

| OMPDC | $k_{cat}$ ($s^{-1}$) | $K_M$ (μM) | $k_{cat}/K_M$ ($M^{-1}s^{-1}$) | $k_{ex}$ ($s^{-1}$) |
|---|---|---|---|---|
| WT | 4.0 | 1.6 | $2.0 \times 10^6$ | 0.015 ± 0.004 |
| I96T | 0.69 ±0.05 | 2.3 ± 0.06 | $3.0 \times 10^5$ | 0.0047 ± 0.0004 |
| I96S | 0.011 ± 0.002 | 1.0 ± 0.04 | $1.0 \times 10^4$ | 0.006 ± 0.001 |
| L123N | 0.64 ± 0.01 | 3.5 ± 0.2 | $1.9 \times 10^5$ | 0.0007 ± 0.0001 |
| L123S | 0.36 ± 0.04 | 3.0 ± 0.5 | $1.2 \times 10^5$ | 0.00039 ± 0.00001 |
| V155S | 0.011 ± 0.003 | 4.7 ± 0.4 | $2.2 \times 10^4$ | 0.006 ± 0.003 |
| V155D | 0.0005 ± 0.0002 | 4.6 ± 0.5 | $4.6 \times 10^2$ | 0.057 ± 0.002 |

**Table 3**. Kinetic parameters for polar substitutions into hydrophobic pocket. All mutants diminished decarboxylation without altering $K_M$ significantly, but highlighted are mutants that decrease decarboxylation without large changes in the rate of H6 exchange.

In crystal structures with the inhibitor BMP, the mutant polar pocket enzymes display active sites that are extremely similar to wildtype OMPDC despite the large differences in $k_{cat}$. The bound ligand and essential residues outside the pocket are completely superimposable on wildtype and pocket-forming residues are virtually undisturbed except for the mutations themselves (Fig. 10). Two conserved water molecules near O4 and C6 appear to be the most mobile elements, and L123S coordinates a third water inside the cavity. The BMP structures validate the hypothesis that the diminished $k_{cat}$ values are attributable to the loss of hydrophobicity, since the introduced polar residues modify the electronic environment without

disrupting architectural features. The polar pocket residues do not collapse the pocket, but satisfy part of their hydrogen bonding imperative by bond formation to the OMP carboxylates that coordinate the carboxylate but ultimately block decarboxylation.

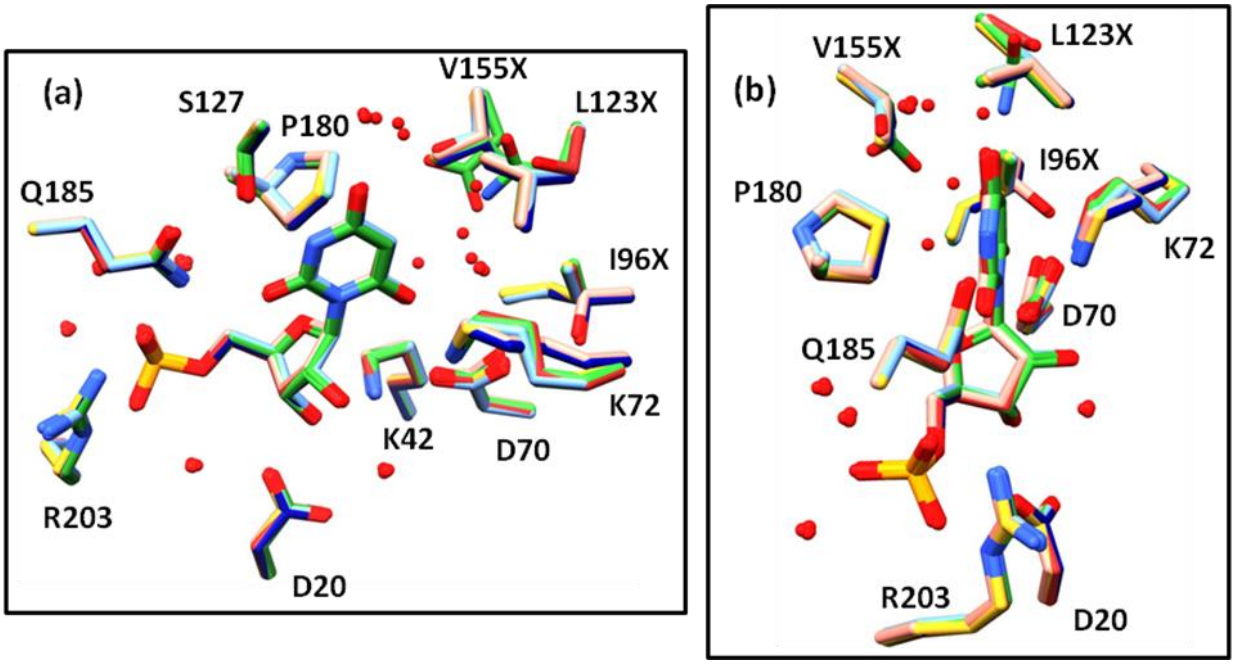


**Figure 10**: Overlay of BMP co-crystallized wildtype OMPDC (goldenrod) and pocket mutantsI96S (salmon), I96T (navy blue), L123S (forest green), L123N (firebrick), V155S (cornflower blue), and V155D (lime green). Shown are active site residues involved in binding ligands, the hydrophobic pocket and the DxKxxD motif. (a) Typical view oriented down the down the α/β barrel. (b) View along the plane of the BMP pyrimidine ring. The pocket is on the ligand's left and DxKxxD motif on the right.

Alternatively, the movement and/or the addition of water molecules in the pocket region of BMP co-crystal structures may indicate that the polarized pockets stabilize a water molecule within the pocket cavity that inhibits decarboxylation with hydrogen bonds or unfavorable steric interactions with the departing C6 carboxylate. Mutants, such as L123S and L123N, which show

kinetic perturbations, but are too far from the C6 site for efficient interaction with the carboxylate, may recruit waters to the pocket.

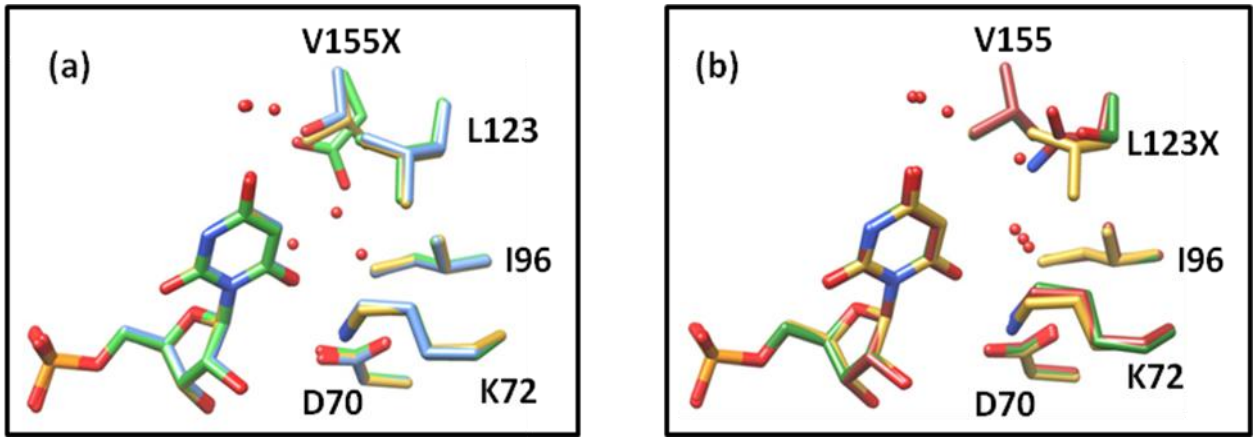


**Figure 11**: Pocket mutants co-crystallized with BMP superimposed over wildtype (goldenrod). Only pocket waters show significant displacement within the active site. (a)Mutant V155S (cornflower blue) and V155D (lime green) with wildtype.(b) Mutant L123S (forest green) and L123N (firebrick) with wildtype.

The polar side-chains of the V155 and L123 mutations are within hydrogen bonding distance (< 3 Å) of the C6 water, which might mimic the position of the carboxylate oxygens (Fig. 11). Thus V155D, V155S, L123S and L123N might stabilize the ground state through new bonds between the carboxylate, enzyme and possibly waters. These interactions lessen the hypothesized strain conducive to decarboxylation. However, hydroxyls of I96S and I96T are not optimally positioned toward C6 (the distance between side-chain hydroxyl and O6 is 6Å (Fig. 12), but instead are oriented away from the pocket cavity. Based upon the BMP structures, I96 mutant hydroxyls may prefer to form hydrogen bonds to D70. These mutants are not forming additional stabilizing carboxylate contacts as other pocket mutants are, but perhaps are acting as hydrogen bond donors to D70. Ultimately I96S and I96T have the same effect as other polar

pocket mutants, but might impair the destabilization imparted by the D70 negative charge rather than stabilizing the substrate directly.

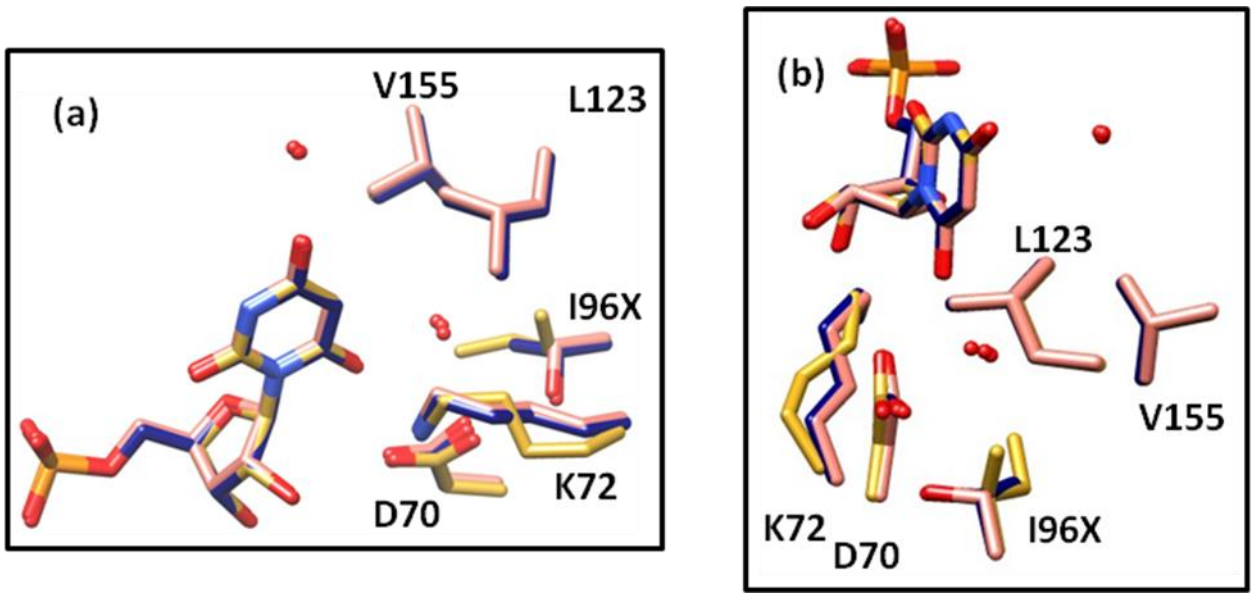


**Figure 12**: A structural comparison of wildtype (goldenrod) and I96S (salmon) and I96T (navy blue) mutants co-crystallized with BMP. I96 mutants may neutralize ground state destabilization by either stabilizing the OMP carboxylate or the nearby D70 carboxylate. (a) Typical view oriented down the α/β barrel. (b) Top view of the active site and pocket, highlighting the relative proximity between I96 mutant side chains and D70, in contrast to I96 and ligand C6.

To investigate potential cooperativity between electrostatic repulsion and I96S or I96T, the kinetics of the double mutant D70N I96S and D50N V155S were measured. Pocket mutants that impair catalysis by thwarting D70 destabilization would have kinetic parameters similar to the D70 mutation alone. A feature that affects only the aspartate should have no effect when the aspartate is replaced. However, both double mutations expressed fully multiplicative $k_{cat}$ effects, indicative of independent mechanisms (Table 4).

The absence of interaction between pocket mutants and the DxKxxD motif corroborates H6 exchange observations. If I96 mutants formed hydrogen bonds with D70, H6 exchange kinetics might be expected to increase as the exchange rate is limited by the rotation rate of K72, which is slowed by its electrostatic attraction to D70. Introducing interactions between a serine or threonine and D70 would diminish the interaction strength between D70 and K72 and consequently enhance rotation and exchange rates. However, the exchange rates of the I96 mutants are identical to the V155S rate.

In spite of five orders of magnitude decrease in their decarboxylation rate, the double mutants D70N I96S and D70N V155S experience less than a ten-fold decrease in exchange rates, providing evidence that though separate, the hydrophobic pocket and electrostatic repulsion induce productive strain on the same pre-transition states during decarboxylation.

| | **Single mutations** | | **Double mutations** | | |
|---|---|---|---|---|---|
| | **$k_{cat}$ ($s^{-1}$)** | **$k_{exchange}$ ($s^{-1}$)** | **projected $k_{cat}$ ($s^{-1}$)** | **$k_{cat}$ ($s^{-1}$)** | **$k_{exchange}$ ($s^{-1}$)** |
| WT | 4.0 | 0.015 | -- | -- | -- |
| D70N | 0.024 (200) | 0.005 (3) | -- | -- | -- |
| I96S | 0.011 (400) | 0.006 (3) | 0.0003 | 0.00006 (**5**) | 0.002 (8) |
| V155S | 0.011 (400) | 0.006 (3) | 0.0003 | 0.00018 (**1.5**) | 0.002 (8) |
| L123S | 0.36 (10) | 0.0004 (40) | 0.009 | 0.00093 (**10**) | 0.00001 (1100) |

**Table 4:** A comparison of single mutations of pocket and D70N mutations to double mutations. In parenthesis are the decreases in rate compared to wildtype. In bold parenthesis are the decreases in rate compared to the *projected* rates for fully multiplicative effects. D70N I96S and D70N V155S are essentially multiplicative in nature.

A subset of these hydrophobic pocket mutants consistently presented diminished exchange rates as well as decarboxylation rate decreases. Unlike the most of the pocket mutants, this group weakens or hinders effective transition state stabilization. To reveal any binding

differences caused by a *hydrophilic* pocket, I tested the inhibition of azauridine 5'-monophosphate (azaUMP) of the pocket mutants and D70N. Compared to wildtype or other pocket mutants, the anomalous L123 mutants also display tighter binding of azaUMP (Fig. 13).

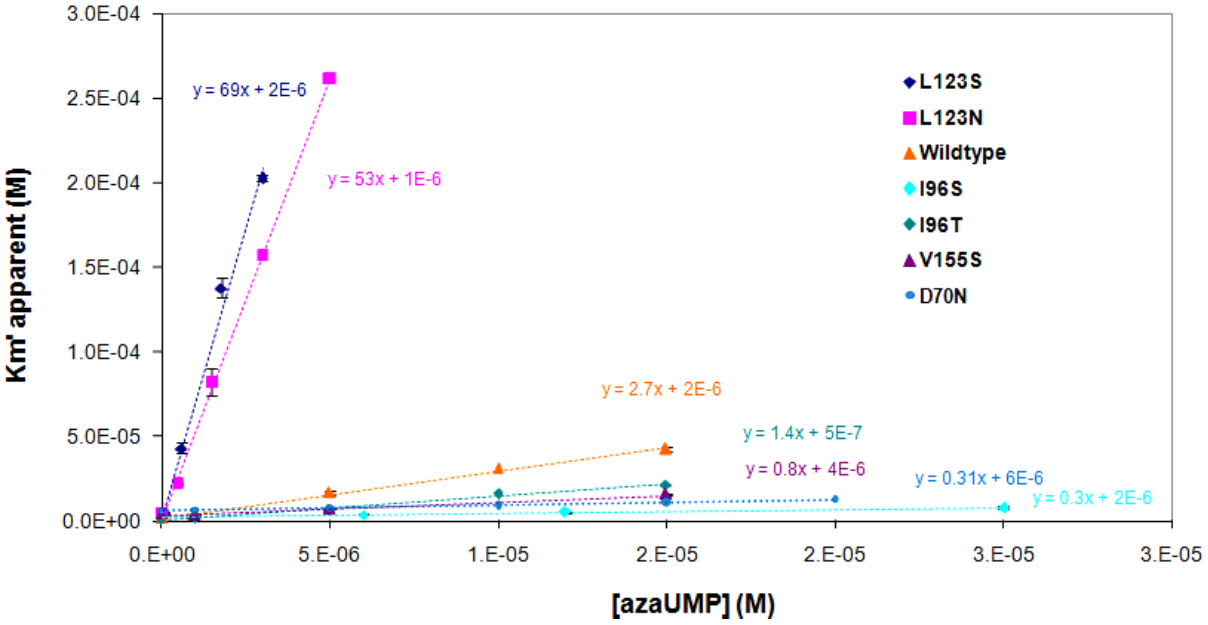


**Figure 13**: AzaUMP inhibition of wildtype and mutants. The mutants form two trends: L123S (navy blue) and L123N (pink), which exhibit heightened azaUMP inhibition, while the other mutants shown decreased inhibition compared to wildtype OMPDC (orange).

| OMPDC | $K_M$ (μM) | $K_i$ (μM) | $(K_i)_{WT}/(K_i)_{mut}$ | $K_M/K_i$ | $(K_M/K_i)_{mut}/(K_M/K_i)_{WT}$ |
|---|---|---|---|---|---|
| WT | 1.4 ± 0.3 | 0.6 | 1.0 | 2.7 | 1 |
| I96T | 1.1 ± 0.4 | 0.76 | 0.8 | 1.4 | 0.5 |
| I96S | 1.7 ± 0.3 | 5.7 | 0.1 | 0.3 | 0.1 |
| V155S | 4.7 ± 0.4 | 5.2 | 0.1 | 0.8 | 0.3 |
| L123S | 3.0 ± 0.6 | 0.043 | 14 | 69 | 30 |
| L123N | 4.4 ± 0.3 | 0.085 | 7 | 53 | 22 |
| D70N | 5.5 ± 0.2 | 18 | 0.03 | 0.3 | 0.1 |

**Table 5**: Comparison of mutant $K_M$ and azaUMP $K_i$ values. $\mathbf{(K_i)_{WT}/(K_i)_{mut}}$ shows the differences in $K_i$, $\mathbf{K_M/K_i}$ corrects the inhibition factor by accounting for binding differences between

mutants, $\mathbf{(K_M/K_i)_{mut}/(K_M/K_i)_{WT}}$ shows the relative inhibition effects with different $K_M$ accounted for.

The $K_i$ of L123 mutants are approximately 10-fold greater than wildtype; however, if $K_M$ values are taken account—slightly elevated compared to wildtype—the relative inhibition increases to 25-fold (Table 5). Subsequent crystal structures produced by the Almo laboratory at the Albert Einstein College of Medicine showed that pocket mutants, like earlier crystal structures of D70 and D75 mutants, bind azaUMP in the *anti*-conformation (Fig. 14). AzaUMP typically binds to wildtype and most active site mutants in the *syn*-conformation to take advantage of the "active site clamp" to achieve favorable enzyme contacts to O2, N3 and O4 of azaUMP. Consequently, the proper reference for pocket mutant inhibition constants is not wildtype OMPDC, but D70 or D75 mutations. Compared to D70N, L123 mutants have 200-fold improved inhibition.

The origin of L123 mutants' tighter binding of azaUMP, and presumably their anomalous exchange rate, might lie in the water maps shown by crystallography. D70 and D75 mutants lack an "active site clamp" that helps hold the pyrimidine ring in position; however, converting the pocket to a more hydrophilic cavity permits ordered waters to solvate azaUMP O2, N3 and O4; the pocket mutants generate a pseudo-active site clamp. The consequence of the water clamp is two-fold: the waters in V155S, I96S and I96T upset L123 geometry. In light of *M. thermoautotrophicum* OMPDCs near imperturbable active site, these small changes might indicate substantial enzyme "discomfort". In contrast, L123 mutants waters are perfectly aligned to facilitate simultaneous bonds to enzyme and ligand.

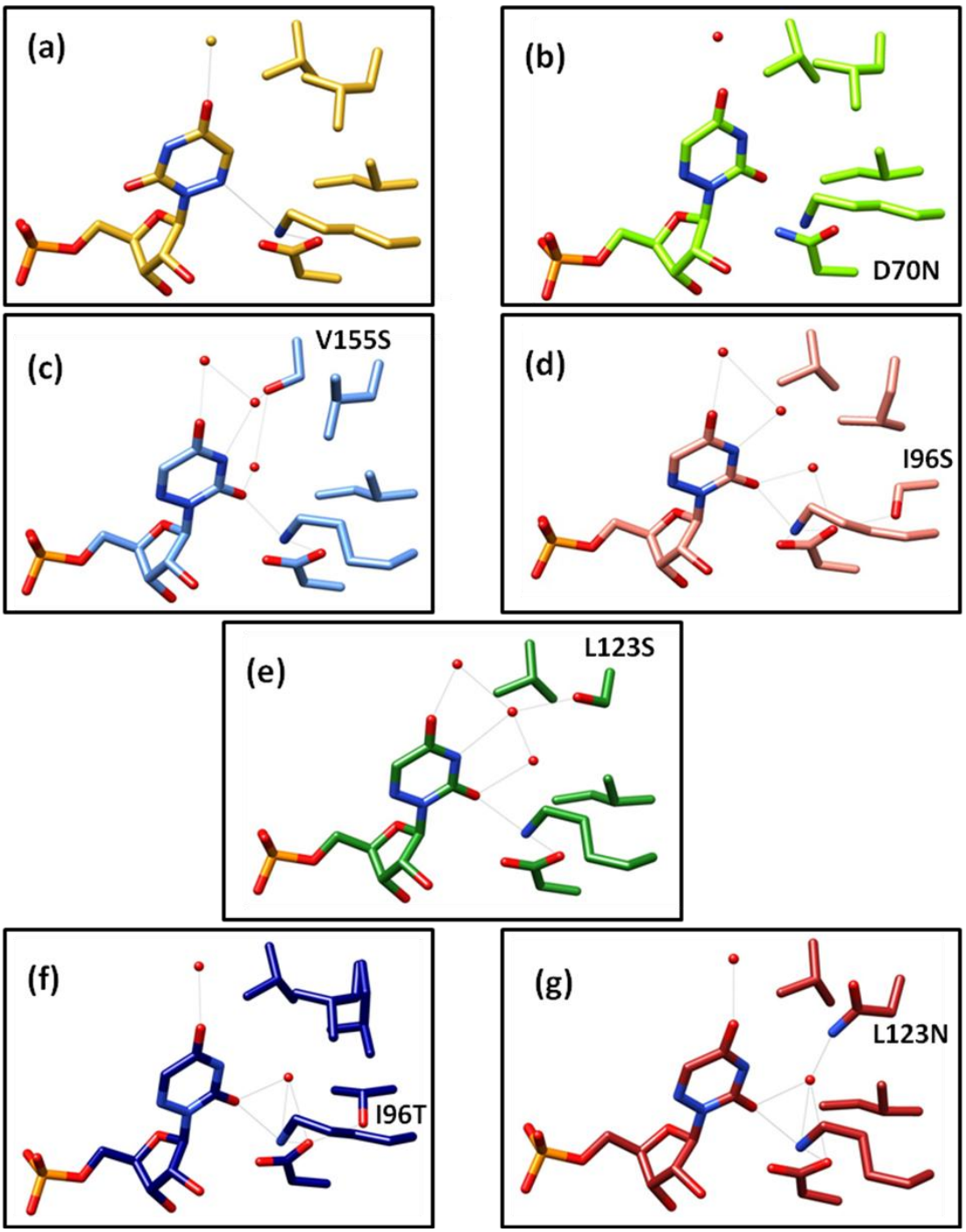


**Figure 14**: OMPDC pocket mutants co-crystallized with azaUMP. In light gray are hydrogen-bonding networks within the pocket and D70 and K72. (a) wildtype OMPDC [pdb file 3g1a], (b)

D70N [pdb file 3g24], (c)V155S, (d) I96S, (e) L123S, (f) I96T, (g) L123N. Gray lines indicate hydrogen bonding networks predicted by Chimera.

Pocket mutants L123S, I96S, and V155S hold two extra ordered waters, whereas I96T and L123N have only one. The number of "clamp" waters in the azaUMP structures has no correlation to the azaUMP inhibition constants; L123N and L123S which exhibited the unexpectedly low $K_i$ values have one and two waters respectively. Rather, binding strength probably reflects pocket residue geometry and the efficacy of the hydrogen bonding networks involved in water and ligand binding.

Decreasing decarboxylation rates with static exchange rates for I96 and V155 mutants provide evidence that hydrogen bond partners stabilize pre-transition states of OMP decarboxylation. The slow exchange, elevated azaUMP inhibition, and azaUMP and BMP waters maps for L123 mutants indicate that these mutants worked differently. Based upon the favorable water contacts found in the crystal structures, L123 mutants may be able to incorporate a pocket water molecule into the active site.

L123 mutants bind azaUMP 200-fold more tightly, but their $K_M$ values are altered by only two or three -fold. The decarboxylation rate, $k_{cat}$, is only mildly affected (around 8-fold) although exchange drops by a factor of 21 to 39. A possible explanation for these incongruities is that mutants containing these extra waters do not productively bind OMP, i.e. decarboxylation cannot occur because of the steric and electronic effects of a water crowding the cavity. Since such a water-bound enzyme may be inactive for decarboxylation, the effective concentration of OMPDC is lowered, which consequently increases $K_{M.}$ L123 mutants show a $K_M$ multiplied by a factor of 2-3. L123 mutants without the rogue water function almost as wildtype, experiencing only a ca. 8-fold decrease in $k_{cat}$, which could be attributed to active site substitution effects. The

conversion of L123 to serine could have a smaller $k_{cat}$ effect than the analogous V155 or I96 substitutions because the L123S side chain is comparatively deeper within the pocket, precluding effective hydrogen bonds the OMP carboxylate.

Because FUMP has no C6 substituent, exchange may continue in the presence of extra waters, albeit at a decreased rate due to altered electronic and steric conditions near the pocket and DxKxxD motif. Similarly, azaUMP has no C6 substituents, which allows the ligand to exploit the pocket waters and flip to a more favorable ring conformation that leads to tight binding for L123 mutants.

The hydrophobic pocket was also explored with a second, more subtle mutagenesis approach, which added bulkier hydrophobic residues into the cavity to retard effective destabilization (Fig. 9). Adding steric hindrance could close off the so-called "$CO_2$ binding site" and prevent the substrate carboxylate from being moved out of the aromatic plane or pushed into the greasy pocket. Simultaneously it would preserve the effects of hydrophobicity. Bulk was added by single or double replacements of small pocket residues with leucines or isoleucines. These mutants have yielded wildtype-like kinetic parameters (10-fold or less differences, Table 6). The incorporation of phenylalanines, in contrast, exhibited drastically altered kinetics for decarboxylation, binding and exchange.

| **OMPDC** | $k_{cat}$ **($s^{-1}$)** | $K_M$ **(μM)** | $k_{cat}/K_M$ **($M^{-1}s^{-1}$)** | $k_{ex}$ **($s^{-1}$)** |
|---|---|---|---|---|
| WT | 4.0 | 2.0 | $2.0 \times 10^6$ | 0.015 ± 0.004 |
| V155I | 1.7 ± 0.1 | 1.0 ± 0.2 | $1.7 \times 10^6$ | 0.010 |
| I96L | 0.24 ± 0.06 | 0.52 ± 0.03 | $4.6 \times 10^5$ | 0.011 ± 0.002 |
| I96L/V155I | 1.9 ± 0.03 | 1.1 ± 0.08 | $1.7 \times 10^6$ | 0.012 |
| V155F | 0.0082 ± 0.0002 | 58 | $1.4 \times 10^2$ | 0.000011 |
| I200F | 0.063 ± 0.002 | 110 | $5.7 \times 10^2$ | 0.0000075 |

**Table 6:** Filling the pocket by replacement of pocket residues with bulkier hydrophobic residues.

Published crystal structures and inhibition constants suggest that the pocket is able to accommodate variously sized C6 functionalities: carboxylates, phosphonates, sulfonates, cyanide and extra water molecules. Perhaps predictably, mutations to leucine and isoleucine apparently are not large enough to perturb the pocket cavity. Phenylalanines, in contrast, appear to be too large or inappropriately oriented and actually impede both substrate binding and catalysis, possibly by forcing the nucleotide into less productive conformations. As H6 exchange is significantly reduced, phenylalanines affect more than pre-transition states of decarboxylation.

## 3.3 CONCLUSIONS

A pocket adjacent to the active site composed of hydrophobic side chains was predicted to partially destabilize the substrate within the active site to promote OMPDC catalysis. Polar substitutions of pocket residues estimate the contribution of hydrophobicity to destabilization and catalysis, while the second approach described, bulk substitution, reflects the degree that the enzyme employs the cavity space itself—e.g. a space to "push" the carboxylate into and/or out of the aromatic plane. Polar residues unambiguously decrease the reaction rate, so the enzyme clearly exploits hydrophobicity to assist decarboxylation. The necessary size of the pocket is less straightforward because of the lack of intermediate sized and shaped residues to sufficiently probe the pocket.

The hydrophobic cavity demonstrated an effect upon the decarboxylation capacity of OMPDC, but little alteration for exchange, which is characteristic of pre-transition state strain. Simultaneously, mutation of this pocket does not alter the enzyme's affinity for the substrate. Crystal structures exhibit active sites residues bound to the transition state analogue BMP that are virtually superimposable with wildtype, supplying further evidence that transition state

stabilization effects or structures are unaltered. These results suggest that the pocket residues decrease the activation barrier by exclusive destabilization of the pre-transition state enzyme-substrate complexes.

Kinetic analyses of D70, an essential OMPDC residue, and hydrophobic pocket mutants demonstrate that both of these architectures generate similar destabilization of the substrate-bound enzyme. The charged OMP carboxylate is strained by hydrophobic residues on one side and electrostatic repulsion on the other. Cumulative effects on decarboxylation show that these means of destabilization work as distinct mechanisms. Consequently, in spite of suggestive crystallographic evidence, D70 does not push the charged carboxylate into the pocket. Although this result does not disallow carboxylate bending, as proposed by reports that the enzyme stabilizes distorted C6 substituents, the impetus for the substrate to overcome both aromatic resonance and hydrophobic repulsion in order to bend is unclear.

Computational modeling in low dielectric environments and non-enzymatic decarboxylation in organic mediums have long shown that the sluggish rate of uncatalyzed OMP decarboxylation originates from the strong solvating power of water. Hydrogen bonds to the carboxylate so stabilize OMP that $\Delta\Delta G$ between reactant and intermediate is staggeringly large compared to most non-cofactor assisted enzymes. Although not the only basis for an acceleration of seventeen orders of magnitude, OMPDC responds to the thermodynamic disadvantage of aqueous or aqueous-like environments. The enzyme active site evolves many favorable contacts to substrate, but also engineers a hydrophobic pocket immediately next to the carboxylate, which I have demonstrated to be valuable for catalysis in this thesis.

# CHAPTER 4: MATERIALS AND METHODS

*OMPDC Site-Directed Mutagenesis, Expression and Purification.* OMPDC from *Methanothermobacter thermoautotrophicus* was cloned into a pET15b vector to use as a template for site-directed mutagenesis. Mutations were incorporated into OMPDC by the overlap extension procedure. Primers containing the desired mutant codons were synthesized by Eurofins MWG Operon. In the initial step, PCR reactions with the mutant primers generate OMPDC sequence in two halves: GerltT7pro and the mutant-containing reverse primers yield the beginning of the sequence to the mutation site, while GerltT7term and the mutant-containing forward primers yield the sequence from the mutation site to the end of the sequences. The sequences were amplified under the following PCR conditions: 1X Taq buffer (Invitrogen), 4 mM $MgCl_2$, 0.8 mM dNTPs, 30 pmol template, 0.4 μM of each primer and 2.5 U native *Pfu* polymerase (Stratagene) and brought to a final volume of 50 μL with Millipore-ultrafiltered water. *PCR program*: 4 min at 95°C, followed by 25 cycles of 45 seconds at 95°C, 30 seconds at 54°C, 135 seconds at 72°C, then 72°C for 7 minutes. The products were checked and purified by 1% agarose gels stained with ethidium bromide. The two half genes, which overlap at the mutation site, were used as templates for PCR to generate the full length gene. The PCR conditions for the full length gene used1X Taq buffer, 4 mM $MgCl_2$, 0.8 mM dNTPs, 5 μL of each half genes, and 2.5 U native *Pfu* polymerase.

The PCR product and pET15b template were separately digested by *Nde* I (Promega) for approximately 16 hours at 37°C and *Bam* HI (Promega) for 3.5 hours at 37°C. The double-digested pET15b template was treated with calf intestinal alkaline phosphatase (Stratagene) for two hours at 37°C to prevent religation of the vector to itself. Insertion of the gene into the pET15b vector was achieved using buffered T4 DNA ligase (Promega) for 16 hours at 16°C.

1 uL of ligation product was electroporated (1.8 mV) into electrocompetent *E. coli* XL1blue cells. All electrocompetent cells were prepared by inoculating 2 L Luria-Bertoni broth with an overnight six-mL starter culture, growing to log phase ($OD_{600}$ = 0.6), and harvesting the cells. Media was removed from the cells with 1 L and 500 mL ice water washes, 40 mL cold 10% glycerol, and stored at -80°C in 10% glycerol. Electrocompetent cells were checked for ampicillin, kanamycin and chloramphenicol resistance.

DNA was isolated from a six-mL culture of XL1blue cells containing the vector and prepared using the QIAprep Miniprep Kit (Qiagen). DNA sequencing was performed by the University of Illinois Core Sequencing Facility to confirm the mutagenesis product sequence. Verified sequences were electroporated into $pyr^-$ (OMPDC negative) *E. coli* competent cells containing the auxiliary plasmid pTara, which encodes for chlorampheicol resistance and T7 polymerase.

A single colony was selected to inoculate six mL starter cultures containing 100 µg/mL ampicillian, 50 µg/mL kanamycin and 34 µg/mL chloramphenicol. When the cultures became confluent, they were used to inoculate twelve liters of media with the same antibiotic concentrations, which were grown at 37°C and 220 rpm for 14-18 hours. Cells were harvested by centrifuging at 5000 x g at 4°C for 10 minutes. Cells were resuspended in binding buffer (Appendix 5.4) and lysed by pulse sonification for 12 minutes. Cellular debris was pelleted by 31,000 x g centrifugation for 50 minutes and the supernatant was injected onto a 100 mL $Ni^{2+}$ column. His-tagged protein was eluted on an 0- 1.0 M imidazole gradient, collected, and dialyzed twice in 20 mM tris buffer (pH7.9) for a minimum of 3 hours each at 4°C.

The His-tag was removed by a 20-hour incubation with ½-1 U thrombin per milligram of protein at room temperature in phosphate buffer. Complete cleavage was checked by SDS-

PAGE. Protein purification was completed with a Q-sepharose column, a strong anion exchange resin, and the protein was eluted with a 0-1.0 M NaCl gradient. Fractions containing protein, typically eluted at 0.4 M NaCl, were collected and dialyzed twice in 20 mM HEPES buffer (pH7.5), 150 mM NaCl, and 3 mM DTT for a minimum of 3 hours each at 4°C. Amicon with 10,000 MW filters were used to concentrate protein to 12-40 mg/mL, which were subsequently frozen in liquid nitrogen and stored at -80°C.

*1-Ribofuranosylbarbiturate monophosphate (BMP) Synthesis*. BMP was synthesized according to a modified procedure by Levine, Brody and Westheimer.[4] 6 mmol Barbiturate was added to 12 mmol trimethylchlorosilane and 72 mmol hexamethyldisilizane and refluxed for 30 minutes to 2 hours until solution was clear. Excess hexamethyldisilazane was removed by high vacuum rotary evaporation followed by 1 hour under vacuum at 60°C.

The dried crystals were dissolved in dichloroethane and added to 5.5 mmol 1-acetyl-2,3,5-tribenzoylribofuranose and 6 mmol $SnCl_4$. The flask was purged with nitrogen gas and stirred overnight (typically 14 hours at room temperature). The condensation reaction was worked up with saturated sodium bicarbonate and saturated sodium chloride. The organic layer was further purified by filtering through Celite layered over a sintered glass frit filter. TLC (2-propanol/concentrated $NH_4OH/H_2O$, 7:1:2) easily distinguishes between nucleoside ($R_f = 0.7$) barbiturate/silylated barbiturate (0.5), and 1-acetyl-2,3,5-tribenzoylribofuranose (0.9).

Dichloroethane was removed by rotary evaporation and the protected nucleoside was redissolved in methanol. Benzoate protecting groups were either removed by ammonia gas (40 psi) in a Parr shaker for 48-72 hours or by 0.08M methoxide in methanol for 12 hours at room temperature. After deprotection, methanol was evaporated and the nucleoside was purified

by an aqueous work up with ethyl acetate and then loaded onto a 100 mL Dowex AG 50x8 resin ($H^+$ form). Barbiturate ribofuranose was eluted quickly from the column with water the nucleoside-containing fractions were collected, rotary evaporated and lyophilized. Recrystallization in water to remove remaining tribenzoylribofuranose and free ribose.

Phosphorylation was achieved by a modified procedure by Fujita *et al*.[35] 3 mmol Nucleoside was added to chilled phosphorus oxychloride and trimethyl phosphate under $N_2$ and stirred overnight. The clear solution was neutralized to pH8 and diluted in 1.5 L water and loaded onto a Dowex 1x8 ($Cl^-$ form). Nucleotide was eluted with a 500 mL 0 – 0.8 M LiCl gradient. BMP typically elutes around 0.4 M LiCl.

*FPLC nucleotide program*:

0.00 conc %B 0.0; 0.00 mL/min 1.00; 0.00 valve.pos 1.1; 0.00 valve.pos 2.6; valve.pos 3.5; 0.00 port.set 6.1; 0.00 mL/mark 10; 0.00 cm/mL 0.10; 100.00 conc %B 0.0; 600.00 conc %B 100; 650.00 conc %B 100.

BMP NMR ($D_2O$, ppm): 6.05 (d,1H), 4.95 (q, 1H), 4.25 (t,1H), 3.81 (m, 1H), 3.72 (q,1H), 3.58 (q, 1H).

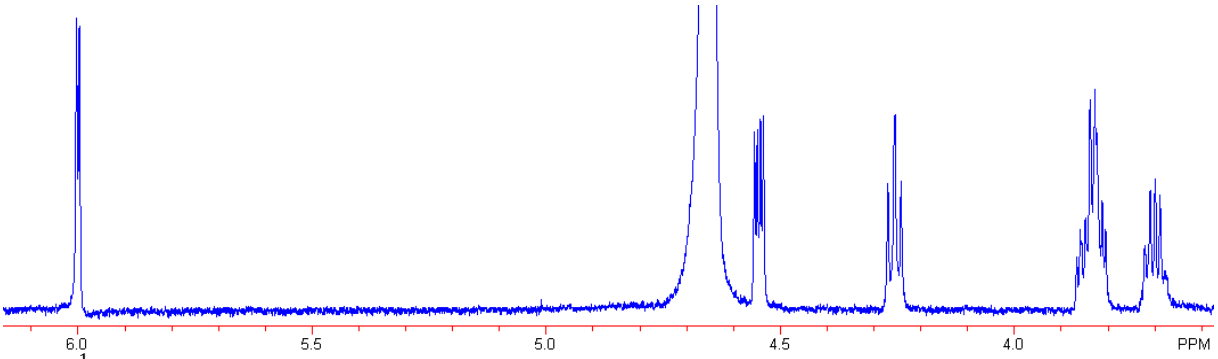

BMP $^1$HNMR spectrum

*3-Deazauridine 5'-monophosphate, 4-deoxy-5-fluorouridine 5'-monophosphate, 4-deoxyuridine 5'-monophosphate.* 6 mmol Base was added to 6.2 mmol trimethylchlorosilane and 30 mmol hexamethyldisilizane and refluxed for 1- 2 hours until solution was clear. Excess

hexamethyldisilazane was removed by high vacuum rotary evaporation followed by 1 hour under vacuum at 60°C.

The dried crystals were dissolved in dichloroethane and added to 5.5 mmol 1-acetyl-2,3,5-tribenzoylribofuranose and 6 mmol $SnCl_4$. The flask was purged with nitrogen gas and stirred overnight (typically 14 hours). The condensation reaction was worked up with saturated sodium bicarbonate and saturated sodium chloride. The organic layer was further purified by filtering through Celite layered over a sintered glass frit filter. 4-Deoxy-5-fluoro-1-(2,3,5-tribenzoyl)uridine was purified with preparative TLC in 3% methanol in dichloromethane.[29] The silica containing nucleoside, which fluoresces a significantly brighter blue than tribenzoylribofuranose, was scraped off the plates and extracted with 5% methanol in dichloromethane. The organic solvent was removed by rotary evaporation and the protected nucleoside was redissolved in methanol.

Benzoate protecting groups were removed by 0.08 M methoxide in methanol for 2-12 hours, stirring at 4°C and then neutralized with Dowex AG 50x8 resin ($H^+$ form) to pH 4. Methanol was evaporated and the nucleoside was purified by an aqueous work up with ethyl acetate, which removed the benzoate ester side product.

UMP derivative nucleotide were phosphorylated according to a modified procedure by Fujita.[35] The nucleoside was added to 3 mole equivalents of chilled phosphorus oxychloride and 22 equivalents trimethyl phosphate under inert nitrogen atmosphere and stirred overnight at 4°C. The clear solution was neutralized to pH8, diluted in 1 L water, and loaded onto a 500 mL DEAE column ($HCO_3^-$ form). The nucleotide was eluted with a 0-0.5 M triethylammonium bicarbonate (pH 8.4) gradient and the fractions containing nucleotide collected. The nucleotide was

repeatedly washed with water and rotary-evaporated to remove excess triethylammonium bicarbonate. Nucleotides were lyophilized and stored at -20°C.

3-DeazaUMP NMR ($D_2O$, ppm): 7.63 (d, 1H), 6.04 (d, 1H), 5.99 (q, 1H), 5.48 (d, 1H slowly exchanges), 4.19 (m, 2H), 4.08 (m, 1H), 3.8-3.9 (m, 2H).

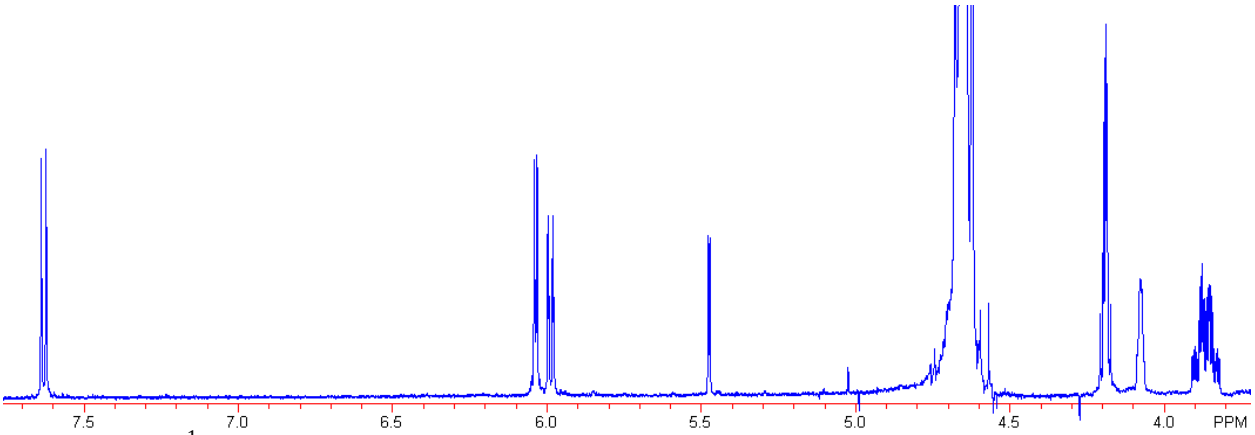


3-DeazaUMP $^1$HNMR spectrum

5-Fluoro-4-deoxyUMP NMR ($D_2O$, ppm): 8.56 (d, 1H), 8.48 (t, 1H) 5.72 (s, 1H), 4.50 (m, 1H), 4.14 (m, 1H), 3.98 (q, 2H).

4-DeoxyUMP NMR ($D_2O$, ppm): 8.6(q, 1H), 8.4 (q, 1H), 6.6 (q, 1H), 5.8 (d, 1H), 4.1 (m, 3H), 4.0 (q, 1H), 3.8 (q, 1H).

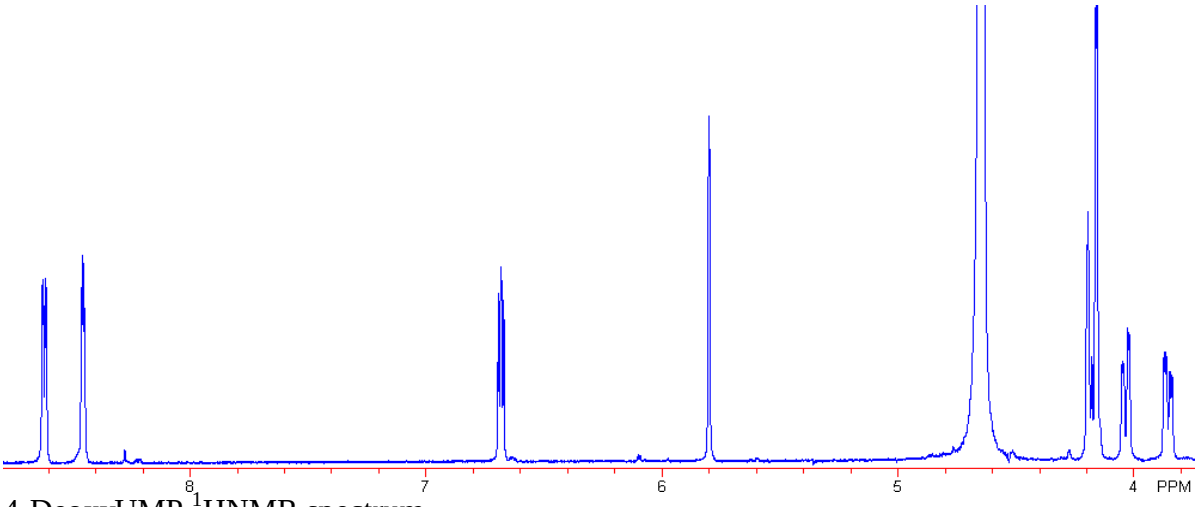


4-DeoxyUMP $^1$HNMR spectrum

*DihydroOMP Synthesis.* DihydroOMP was synthesized according to Chan *et al.* 20mg (0.1µmol) OMP was dissolved in 6 mL 50% aqueous methanol. The reaction was catalyzed by13 mg of 5% palladium over activated carbon and pressurized with 40 psi hydrogen gas for 24-48 hours at room temperature. The catalyst was removed by filtering through Celite over a coarse fritted filter and washed with water. The product was lyophilized to dryness and stored at -20°C.

*FUMP and OMP Synthesis*. FUMP was synthesized according to a modified procedure by Fujita *et al*.[35] 1.9 mmol 5-Fluorouridine (purchased from Sigma Aldrich) was added to chilled phosphorus oxychloride and trimethyl phosphate under $N_2$ and stirred overnight. The clear solution was neutralized to pH8, diluted in 1 L water, and loaded onto a 500 mL DEAE column ($HCO_3^-$ form). The nucleotide was eluted with a 0-0.5 M triethylammonium bicarbonate (pH 8.4) gradient and the fractions containing FUMP collected. Repeated water washes and rotary evaporations were remove excess triethylammonium bicarbonate from FUMP fractions.

OMP was synthesized with 1-phosphoribosylpyrophosphate and orotate, which were purchased from Sigma Aldrich, using OPRTase according to a procedure from Kui Chan's thesis.

*Decarboxylation Assay: Initial Rates.* The rate of decarboxylation, $V_{max}$, was monitored spectrophotometrically on a Perkin Elmer Lambda 14 UV/Vis spectrophotometer at 279 nm with increasing substrate concentration until saturation. The Michaelis-Menton constant, $K_M$, was calculated as the substrate concentration at half the maximal velocity. Because the substrate OMP, product UMP and the enzyme absorb at 279 nm, the assay wavelength and $\Delta\varepsilon$ were

adjusted at OMP concentration greater than 120 μM to prevent absorbance values greater than 1 (Appendix 5.2.2).

*Decarboxylation Assay: First Order Decay.* The rate of decarboxylation, $V_{max}$, for enzymes exhibiting wildtype-like kinetics was measured spectrophotometrically at 279 nm ($\varepsilon = 2400\ M^{-1}$) by saturating the enzyme with OMP amounts greater than 10-fold the $K_M$ value. The $K_M$ values of OMPDC are approximately 1.5 μM, which cannot be accurately quantitated by initial velocities; $K_M$ values were measured by the first order decay of the OMPDC reaction, wherein the change in absorbance over time, at substrate concentrations ≤ 20 % of the estimated $K_M$, was fitted to the following first order decay equation

$$A = Af + (Ai - Af)e^{-kt}$$

where t is time, A is the absorbance at time t, Af is the absorbance after reaction completion, Ai is the calculated initial absorbance, and *k* is the first order rate constant equal to $V_{max}/K_M$. The amount of OMP added to the assay was calculated to ensure saturation, however, the product UMP introduces a small amount of error as it has a $K_i$ of 170 μM. Therefore OMP concentrations greater than 10-fold $K_M$ were not applied to first order decay assays.

*Exchange Assay*. Exchange of the H6 proton of FUMP was measured by the rate of incorporation of solvent-derived deuterium. FUMP (triethylammonium salt) was lyophilized to dryness and resuspended in deuterium oxide. The concentration of FUMP was determined at 269 nm (ε=9200). The rate of deuterium incorporation was observed at 25°C by pre-acquisition decay array by NMR with 150 transients (20 minutes) per timepoint, a sweep width of 950 Hz, a relaxation time of 2 microseconds, and an acquisition time of 6 microseconds. $^{19}$F-NMR shows

well-resolved peaks for protonated FUMP (hFUMP, doublet of doublets) and deuterated FUMP (dFUMP, doublet) shifted downfield by 0.28 ppm. A typical exchange reaction with 0.5 mg/mL wildtype OMPDC enzyme exchanges approximately 50% of 5 mM FUMP in 3 hours. Enzyme stored in protonated solvents were washed with buffered deuterium oxide in 150 uL Amicon centrifuge tubes with a 10,000 Da molecular weight filter. The exchange reaction was performed at 25 C in deuterium oxide buffered with 100 mM glycylglycine (pD 9.35) solution that maintained an ionic strength of 0.1 M with NaCl.

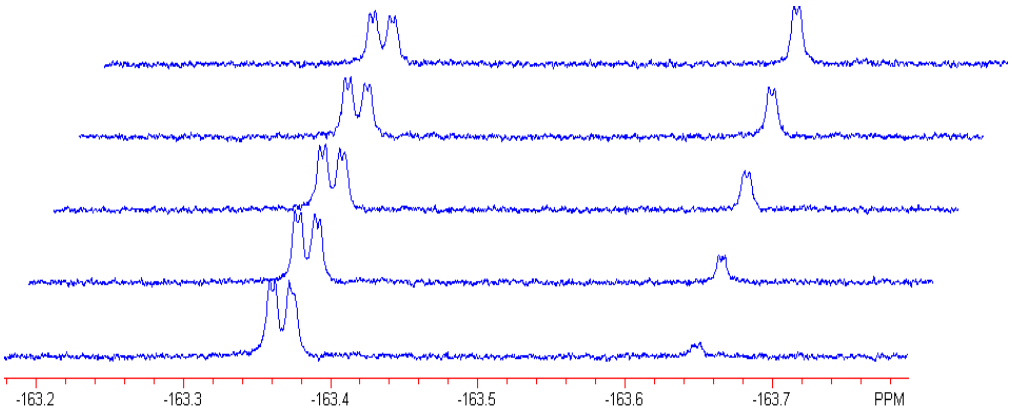


Representative H6 exchange reaction in $D_2O$. hFUMP, the doublet of doublets at -163.37 ppm, is exchanged to dFUMP, the doublet at -163.65 ppm.

The exchange rate was measured by comparing the integration of hFUMP to the combined integration of hFUMP and dFUMP and plotted against time. The observed exchange rate, $k_{obs}$, was given by the negative slope of the linear fitted line and the exchange rate, $k_{ex}$, was calculated by

$$k_{ex} = k_{obs}[\text{total FUMP}]/[\text{OMPDC}]$$

where [hFUMP + dFUMP] is the total FUMP concentration and [OMPDC] is the total enzyme concentration.

*6-AzaUMP, 3-DeazaUMP, UMP, 4-Deoxy-5-fluoroUMP Inhibition.* Inhibition constants were measured by first order decay with inhibitor concentrations, which yields the apparent Michaelis-

Menton constants, $K_M$'. The range of inhibitor concentrations was taken close to the $K_i$ values thus, azaUMP concentrations were between 0.1 and 30 μM while 3-deazaUMP and UMP were measured between 10 and 120 μM. However, as inhibitors absorb at 279 nm, inhibitor concentrations greater than 150 μM had poor signal to noise. Thus, the inhibition of DFUMP could not be measured as it exceeded the range of the assay. The slope of equation

$$K_M' = K_M (1 + [I] / K_i)$$

is $K_M/K_i$, where [I] is the inhibitor concentration, and which yields the inhibition constant, $K_i$.

REFERENCES


(1) Radzicka, A.; Wolfenden, R. *Science* **1995**, *267*, 90-93.

(2) Miller, B. G.; Butterfoss, G. L.; Short, S. A.; Wolfenden, R. *Biochemistry* **2001**, *40*, 6227-6232.

(3) Amyes, T. L.; Richard, J. P.; Tait, J. J. *Journal of the American Chemical Society* **2005**, *127*, 15708-15709.

(4) Levine, H. L.; Brody, R. S.; Westheimer, F. H. *Biochemistry* **1980**, *19*, 4993-4999.

(5) Poduch, E.; Bello, A. M.; Tang, S.; Fujihashi, M.; Pai, E. F.; Kotra, L. P. *J Med Chem* **2006**, *49*, 4937-4945.

(6) Lewis Jr, C.; Wolfenden, R. *Biochemistry* **2007**, *46*, 13331-13343.

(7) Thirumalairajan, S.; Mahaney, B.; Bearne, S. L. *Chemical Communications* **2010**, *46*, 3158-3160.

(8) Traut, T. W.; Temple, B. R. S. *Journal of Biological Chemistry* **2000**, *275*, 28675-28681.

(9) Barnett, S. A.; Amyes, T. L.; Wood, B. M.; Gerlt, J. A.; Richard, J. P. *Biochemistry* **2008**, *47*, 7785-7787.

(10) Chan, K. K.; Wood, B. M.; Fedorov, A. A.; Fedorov, E. V.; Imker, H. J.; Amyes, T. L.; Richard, J. P.; Gerlt, J. A. *Biochemistry* **2009**.

(11) Silverman, R. B.; Groziak, M. P. *Journal of the American Chemical Society* **1982**, *104*, 6436-6439.

(12) Van Vleet, J. L.; Reinhardt, L. A.; Miller, B. G.; Sievers, A.; Cleland, W. W. *Biochemistry* **2008**, *47*, 798-803.

(13) Acheson, S. A.; Bell, J. B.; Jones, M. E.; Wolfenden, R. *Biochemistry* **1990**, *29*, 3198-3202.

(14) Appleby, T. C.; Kinsland, C.; Begley, T. P.; Ealick, S. E. *Proceedings of the National Academy of Sciences U.S.A.* **2000**, *97*, 2005-2010.

(15) Begley, T. P.; Appleby, T. C.; Ealick, S. E. *Curr. Opin. Struct. Biol.* **2000**, *10*, 711-718.

(16) Ehrlich, J. I.; Hwang, C. C.; Cook, P. F.; Blanchard, J. S. *Journal of the American Chemical Society* **1999**, *121*, 6966–6967.

(17) Toth, K.; Amyes, T. L.; Wood, B. M.; Chan, K.; Gerlt, J. A.; Richard, J. P. *Journal of the American Chemical Society* **2007**, *129*, 12946–12947.

(18) Beak, P.; Siegel, B. *Journal of the American Chemical Society* **1976**, *98*, 3601.

(19) Lee, J. K.; Houk, K. N. *Science* **1997**, *276*, 942-945.

(20) Harris, P.; Poulsen, J.-C. N.; Jensen, K. F.; Larsen, S. *Biochemistry* **2000**, *39*, 4217-4224.

(21) Wu, N.; Mo, Y.; Gao, J.; Pai, E. F. *Proceedings of the National Academy of Sciences U.S.A.* **2000**, *97*, 2017-2022.

(22) Miller, B. G.; Hassell, A. M.; Wolfenden, R.; Milburn, M. V.; Short, S. A. *Proceedings of the National Academy of Sciences U.S.A.* **2000**, *97*, 2011-2016.

(23) Rishavy, M. A.; Cleland, W. W. *Biochemistry* **2000**, *39*, 4569–4574.

(24) Jencks, W. P. *Advances in Enzymology and Related Areas of Molecular Biology*; J Wiley & Sons, Inc: New York, 1975; Vol. 43.

(25) Warshel, A.; Strajbl, M.; Villa, J.; Florian, J. *Biochemistry* **2000**, *39*, 14728.

(26) Houk, K. N.; Lee, J. K.; Tanillo, D. J.; Bahmanyar, S.; Hietbrink, B. N. *ChemBioChem* **2001**, *2*, 113-118.

(27) Wu, N.; Gillon, W.; Pai, E. F. *Biochemistry* **2002**, *41*.

(28) Albert, A.; Phillips, J. N. *Journal of the American Chemical Society* **1956**, 1294-1305.

(29) Driscoll, J. S.; Marquez, V. E.; Plowman, J.; Liu, P. S.; Kelley, J. A.; Barchi Jr., J. J. *J. Med. Chem.* **1991**, *34*, 3280-3284.

(30) Crosby, J.; Lienhard, G. E. *Journal of the American Chemical Society* **1970**, *92*, 5707-5716.

(31) Gutowski, J. A.; Lienhard, G. E. *Journal of Biological Chemistry* **1976**, *251*, 2863.

(32) Lewis Jr, C.; Wolfenden, R. *Biochemistry* **2009**, *48*, 8738-8745.

(33) Amyes, T. L.; Wood, B. M.; Chan, K.; Gerlt, J. A.; Richard, J. P. *journal of the American Chemical Society* **2008**, *130*, 1574-1575.

(34) Meza-Avina, M. E.; Wei, L.; Liu, Y.; Poduch, E.; Bello, A. M.; Mishra, R. K.; Pai, E. F.; Kotra, L. P. *Bioorg Med Chem* **2010**, *18*, 4032-4041.

(35) Fujita, K.; Matsukawa, A.; Shibata, K.; Tanaka, T.; Taniguchi, M.; Oi, S. *Carbohydr. Res.* **1994**, *265*, 299-302.

(36) Currie, B. L.; Robins, R. K.; Robins, M. J. *Journal of Heterocylic Chemistry* **1970**, *7*, 323-329.

APPENDIX A: EXTINCTION COEFFICIENTS

Nucleotide extinction coefficients ε at wavelength $\lambda_{max}$

| **Nucleotide** | **ε (extinction coefficient, $M^{-1}cm^{-1}$)** | **λ (nm)** |
|---|---|---|
| Orotidine 5'-monophosphate | 9430 | 267 |
| Uridine 5'-monophosphate | 10000 | 262 |
| 5-Fluorouridine 5'-monophosphate | 8000 | 265 |
| 5-Fluoro-4-deoxyuridine 5'-monophosphate | 1720 | 325 |
| 3-Deazauridine 5'-monophosphate[36] | 4260 | 278 |
| Barbiturate 5'-monophosphate | 19700 | 260 |
| **Enzyme** | **ε (extinction coefficient, $M^{-1}cm^{-1}$)** | **λ (nM)** |
| OMPDC | 6085 | 280 |

Extinction coefficients and relative absorbance changes for OMP decarboxylation at pH 7.1

| **λ (nm)** | **Δε at 25°C ($M^{-1}s^{-1}$)** | **$Abs_{OMP}$ relative to 279 nm** | **Δε for reaction relative to 279 nm** |
|---|---|---|---|
| 290 | 1620 | 0.31 | 0.68 |
| 289 | 1775 | 0.36 | 0.74 |
| 288 | 1917 | 0.40 | 0.80 |
| 287 | 2048 | 0.46 | 0.85 |
| 286 | 2158 | 0.51 | 0.90 |
| 285 | 2244 | 0.57 | 0.94 |
| 284 | 2311 | 0.64 | 0.96 |
| 283 | 2358 | 0.70 | 0.98 |
| 282 | 2386 | 0.78 | 0.99 |
| 281 | 2402 | 0.85 | 1.00 |
| 280 | 2409 | 0.92 | 1.00 |
| 279 | 2400 | 1.00 | 1.00 |
| 278 | 2375 | 1.08 | 0.99 |
| 277 | 2327 | 1.15 | 0.97 |

APPENDIX B: PRIMERS, GENE AND PROTEIN SEQUENCES

Primer sequences list

| **Primer** | **Sequence** |
|---|---|
| GerltT7pro | CCCGCGAAATTAATACGACTCACTATAGGGG |
| GerltT7term | CAAGGGGTTATGCTAGTTATTGCTCAGCGG |
| S127P_f | CCTCCTGACAGAGATGCCACACCCAGGG |
| S127P_r | CCCTGGGTGTGGCATCTCTGTCAGGAGG |
| S127G_f | CCTCCTGACAGAGATGGGACACCCAGGG |
| S127G_r | CCCTGGGTGTCCCATCTCTGTCAGGAGG |
| S127A_f | CCTCCTGACAGAGATGGCACACCCGGGGGCAG |
| S127A_r | CTGCCCCCGGGTGTGCCATCTCTGTCAGGAGG |
| V155I_f | GGGTCGATCTTGGTGTCAAAAATTATATTGGCCCATCCACAAGACC |
| V155I_r | GGTCTTGTGGATGGGCCAATATAATTTTTGACACCAAGATCGACCC |
| V155F_f | GGGTCGATCTTGGTGTCAAAAATTATTTTGGCCCATCCACAAGACC |
| V155F_r | GGTCTTGTGGATGGGCCAAAATAATTTTTGACACCAAGATCGACCC |
| V155S_f | GGGGTCGATCTTGGTGTCAAAAATTATTCTGGCCCATCCACAAGACC |
| V155S_r | GGTCTTGTGGATGGGCCAGAATAATTTTTGACACCAAGATCGACCCC |
| V155D_f | GGGGTCGATCTTGGTGTCAAAAATTATGATGGCCCATCCACAAGACC |
| V155D_r | GGTCTTGTGGATGGGCCATCATAATTTTTGACACCAAGATCGACCCC |
| I96L_f | GGCGGGGGCTGATGCCATACTAGTCCACGGATTCCCGGG |
| I96L_r | CCCGGGAATCCGTGGACTAGTATGGCATCAGCCCCCGCC |
| I96F_f | GGCGGGGGCTGATGCCATATTTGTCCACGGATTCCCGGG |
| I96F_r | CCCGGGAATCCGTGGACAAATATGGCATCAGCCCCCGCC |
| I96S_f | GGCGGGGGCTGATGCCATAAGCGTCCACGGATTCCCGGG |
| I96S_r | CCCGGGAATCCGTGGACGCTTATGGCATCAGCCCCCGCC |
| I96T_f | GGCGGGGGCTGATGCCATAACAGTCCACGGATTCCCGGG |
| I96T_r | CCCGGGAATCCGTGGACTGTTATGGCATCAGCCCCCGCC |
| L123N_f | GGGACGTGAGGTCTTCCTCAACACAGAGATGTCACACCCGGGG |
| L123N_r | CCCCGGGTGTGACATCTCTGTGTTGAGGAAGACCTCACGTCCC |
| L123S_f | GGGACGTGAGGTCTTCCTCTCGACAGAGATGTCACACCCGGGG |
| L123S_r | CCCCGGGTGTGACATCTCTGTCGAGAGGAAGACCTCACGTCCC |
| I200F_f | CGCAGATGCCATATTTGTTGGAAGATCCATCTACCTTGCAGATAACCC |
| I200F_r | GGGTTATCTGCAAGGTAGATGGATCTTCCAACAAATATGGCATCTGCG |
| D70A_f | GGCTGCAGAATCATAGCCGCCTTCAAGGTTGCAG |
| D70A_r | CTGCAACCTTGAAGGCGGCTATGATTCTGCAGCC |
| D70N_f | GGCTGCAGAATCATAGCCAATTTCAAGGTTGCAG |
| D70N_r | CTGCAACCTTGAAATTGGCTATGATTCTGCAGCC |

Gene and Protein Sequences

OMPDC DNA sequence

ATGAGATCCCGGAGAGTTGATGTTATGGACGTTATGAACAGACTTATACTTGCAATG
GACCTCATGAACCGGGATGATGCCCTCAGGGTCACCGGAGAGGTCAGGGAATACAT
AGACACGGTCAAGATAGGGTACCCCCTTGTACTCTCAGAGGGTATGGATATCATTGC
TGAGTTCAGAAAGAGATTTGGCTGCAGAATCATAGCCGACTTCAAGGTTGCAGATAT
ACCCGAGACCAATGAAAAGATATGCCGGGCCACCTTCAAGGCGGGGGCTGATGCCA
TAATAGTCCACGGATTCCCGGGAGCAGACAGTGTCAGGGCCTGCCTCAATGTCGCA
GAGGAAATGGGACGTGAGGTCTTCCTCCTGACAGAGATGTCACACCCGGGGGCAGA
GATGTTCATACAGGGCGCTGCAGATGAAATAGCCAGAATGGGGGTCGATCTTGGTG
TCAAAAATTATGTTGGCCCATCCACAAGACCTGAAAGGCTTTCAAGGCTGAGGGAA
ATCATAGGTCAGGATTCATTTCTCATATCCCCCGGTGTGGGAGCCCAGGGAGGAGAC
CCAGGGGAGACCCTCAGGTTCGCAGATGCCATAATAGTTGGAAGATCCATCTACCTT
GCAGATAACCCTGCAGCTGCAGCAGCAGGGATAATAGAATCCATTAAAGACCTTCT
GAATCCCTAA

OMPDC protein sequence

MRSRRVDVMDVMNRLILAMDLMNRDDALRVTGEVREYIDTVKIGYPLVLSEGMDIIAE
FRKRFGCRIIADFKVADIPETNEKICRATFKAGADAIIVHGFPGADSVRACLNVAEEMGR
EVFLLTEMSHPGAEMFIQGAADEIARMGVDLGVKNYVGPSTRPERLSRLREIIGQDSFLIS
PGVGAQGGDPGETLRFADAIIVGRSIYLADNPAAAAAGIIESIKDLLNP*

APPENDIX C: BUFFERS AND AKTA PROGRAMS

Buffers for Nickel Affinity Chromotography

*1x Binding Buffer*: 5 mM imidazole, 500 mM NaCl, 20 mM Tris-HCl (pH 7.9), 5 mM $Mg_2Cl$.
*1x Wash Buffer*: 60 mM imidazole, 500 mM NaCl, 20 mM Tris-HCl (pH 7.9), 5 mM $Mg_2Cl$.
*1x Elute Buffer*: 1 M imidazole, 500 mM NaCl, 20 mM Tris-HCl (pH 7.9), 5 mM $Mg_2Cl$
*1x Charge Buffer*: 50 mM $NiSO_4$.
*1x Strip Buffer*: 100 mM EDTA, 500 mM NaCl, 20 mM Tris-HCl (pH 7.9).

AKTA FPLC Program: Nickel Affinity Chromotography

Resin: Chelating Sepharose Fast Flow (GE Healthcare; 17 0575-01)
Approximate volume: 100 mL

- Load Sample
  Flow 3 mL/min

- Wash Unbound Sample
  Flow 4 mL/min
  0-300 1x binding
  300-600 5% 1x elution, 95% 1x wash
  600-750 1x binding

- Gradient Elution
  Flow 4 mL/min
  Fraction size 10 mL
  750-1200 100% 1x wash – 100% 1x elution

- Clean and Regenerate Column
  1200-1450 1x strip
  1450-1800 water
  1800-2000 1 M NaCl
  2000-2050 water
  2050-2500 1 M NaOH
  2500-2550 water
  2550-2750 50% aqueous ethanol
  2750-2825 water
  2825-3125 1x charge
  3125-3425 1x binding

Buffers for Strong Anion Exchange (Q Sepharose) Chromatography, Thrombin Cleavage, and Storage

*1x Phosphate Buffered Solution*: 137 mM NaCl, 2.7 mM KCl, 10 mM $Na_2HPO_4$, 1.8 mM, $KH_2HPO_4$.

*1x High Salt Buffer*: 1 M NaCl, 20 mM Tris-HCl (pH 7.9).
*1x Low Salt Buffer*: 20 mM Tris-HCl (pH 7.9).
*1x Storage Buffer*: 150 mM NaCl, 20 mM HEPES (pH 7.5), ±3 mM DTT.

AKTA FPLC Program: Strong Anion Exchange Chromatography

Resin: Chelating Sepharose Fast Flow (GE Healthcare; 17 0575-01)
Approximate volume: 100 mL

- Load Sample
  Flow 3 mL/min

- Wash Unbound Sample
  Flow 2 mL/min
  0-135 1x low salt buffer

- Gradient Elution
  Flow
  Fraction size
  135-885 100% 1x low salt – 100% 1x high salt

- Clean and Regenerate Column
  Flow 2 mL/min
  885-950 Water
  950-1150 1 M NaOH
  1150-1250 Water
  1250-1350 50% aqueous ethanol
  1350-1450 Water
  1450-1650 1 M NaCl
  1650-1850 1x low salt